ORIGINAL PAPER

Metasomatic ijolite, glimmerite, silicocarbonatite, and antiskarn formation: carbonatite and silicate phase equilibria in the system Na$_2$O–CaO–K$_2$O–FeO–MgO–Al$_2$O$_3$–SiO$_2$–H$_2$O–O$_2$–CO$_2$

Michael Anenburg[1] · Jesse B. Walters[2,3]

Abstract

Silicocarbonatites are carbonatite rocks containing > 20% silicate minerals. Their formation is not well understood due to low silica solubility in carbonatite melts and negligible amounts of silicate minerals on carbonatite melt cotectics at upper crustal conditions. We explore whether silicocarbonatites can be thought of as antiskarns: rocks formed by leaching of SiO$_2$ from siliceous wall rocks by carbonatite melts, and its deposition as solid silicate minerals by reaction with chemical components already present in the carbonatite melt. Solid state thermodynamic modelling at 1–5 kbar and 500–800 °C predicts that calcite–dolomite–magnetite assemblages will transform to dolomite-free silicocarbonatites with an increase in silica contents. In sodic systems, the formation of aegirine and alkali amphiboles suppresses silica activity despite elevated silica contents. Therefore, dolomite remains stable, but Fe^{3+} is consumed, firstly from magnetite breakdown, and secondly by coupled Fe oxidation and reduction of CO$_2$ to CO, CH$_4$, and graphite, particularly at higher pressures. Despite a net increase in Fe^{3+}/Fe^{2+}, the system evolves to increasingly lower oxygen fugacity. In aluminous systems, nepheline indicates high temperatures whereas alkali feldspars form at lower temperatures. Modelling of potassic systems demonstrates stability of mostly phlogopite-rich biotites, leading to Fe^{2+} increase in all other carbonate and silicate phases. We find that perthites are expected in high pressures whereas two feldspars are more likely in lower pressures.

Aspects of the clinopyroxene natural compositional trend (diopside to hedenbergite to aegirine) of carbonatite systems can be explained by silica contamination. Ferrous clinopyroxenes typically require low alumina and are predicted in potassic or low temperature sodic systems, primarily at mid to high pressures. Silica contamination permits the formation of silicocarbonatite-like assemblages in a way that is not limited by SiO$_2$ solubility in carbonatite melts. Glimmerites and clinopyroxene-rich rocks (such as the ijolite series) that often occur around carbonatite rocks at the contact with silica-oversaturated wall rocks can be explained as the extreme end of silica contamination of carbonatite melts. Therefore, these clinopyroxenites and glimmerites can form solely via metasomatic processes without the presence of a silicate melt.

Keywords Pyroxenite · Alkaline complexes · carbonatite · Carbonatite metasomatism · Antiskarn · Glimmerite · Phlogopitite · Aillikite

Introduction

Silicocarbonatites are defined as containing more than 20% silica (Le Maitre et al. 2002; Mitchell 2005), but their origin is somewhat enigmatic. Silica solubility in carbonatite melts at sub-1000 °C crustal conditions is typically low (Anenburg and Guzmics 2023; Martin et al. 2013; Weidendorfer and Asimow 2022). They are often mineralogically related to silica undersaturated mafic rocks that commonly surround carbonatite rocks in ring complexes. One hypothesis for the origin of these silicate assemblages is that they represent crystallisation products

of immiscible carbonatite–silicate pairs (Kamenetsky et al. 2021; Woolley 2003). Evidence for immiscibility largely lies in observation of immiscible pairs in melt inclusions (Berndt and Klemme 2022; Guzmics et al. 2019, 2015; Mitchell and Dawson 2012; Sharygin et al. 2012; Veksler and Lentz 2006), and abundant experimental evidence for its existence (Brooker and Kjarsgaard 2011; Kjarsgaard and Hamilton 1988; Kjarsgaard et al. 1995; Lee and Wyllie 1998; Martin et al. 2013, 2012; Veksler et al. 2012). However, generalising small scale immiscibility features— whether experimentally or in natural inclusions—to larger occurrences is challenging and a convincing demonstration that any certain alkaline silicate-complex formed by immiscibility is lacking (e.g. Doroshkevich et al. 2017). A second hypothesis suggests that silicate rocks represent cumulate silicate minerals from one or more batches of hot carbonated silicate melts that eventually evolve to carbonatite melts (Doroshkevich et al. 2017; Savard and Mitchell 2021; Woolley 2003; Wu et al. 2017).

A third, relatively new hypothesis is silica assimilation by carbonatite melts (Vasyukova and Williams-Jones 2022). Such melts are increasingly being recognised as metasomatic agents that facilitate chemical exchange between the carbonatite system and its surrounding rocks (Anenburg et al. 2020a; Giebel et al. 2019; Hode Vuorinen and Skelton 2004; Skelton et al. 2007; Vasyukova et al. 2023). The best known of these processes is fenitisation, in which carbonatite-derived alkali fluids migrate to siliceous wall rocks, increasing their Na and K contents, and transforming them into rocks containing a characteristic assemblage of alkali feldspars, micas, aegirine, riebeckite, arfvedsonite, and other alkali-rich minerals (Elliott et al. 2018). Less known are the recently recognised antiskarns, which are rocks that occur within the carbonatite igneous bodies and contain mineral assemblages indicating contamination of the carbonatite melt by externally derived silica (Stoppa 2021; Su et al. 2023). The mineral assemblage observed in antiskarns likely depends on the evolutionary stage of the carbonatite melt (Yaxley et al. 2022). Antiskarns forming from primitive carbonatite melts in which alkalis are yet to be strongly enriched often contain Mg and Ca-silicates typical of traditional skarns such as olivine, diopside, and wollastonite (Bouabdellah et al. 2022; Chmyz et al. 2022; Su et al. 2023). In contrast, antiskarns formed in more evolved and alkali-rich carbonatite systems contain mineral assemblages akin to those observed in the fenites mentioned earlier (Vasyukova and Williams-Jones 2023; Yaxley et al. 2022; Zheng et al. 2023). Although both antiskarns and silicocarbonatites describe silicate rocks or mineral assemblages occurring in carbonatite systems, they do not refer to the same thing. The term "antiskarn" describes the genesis whereas "silicocarbonatite" is descriptive (see Fig. 1 for details). Also note that we only consider silicocarbonatites as those rocks in which
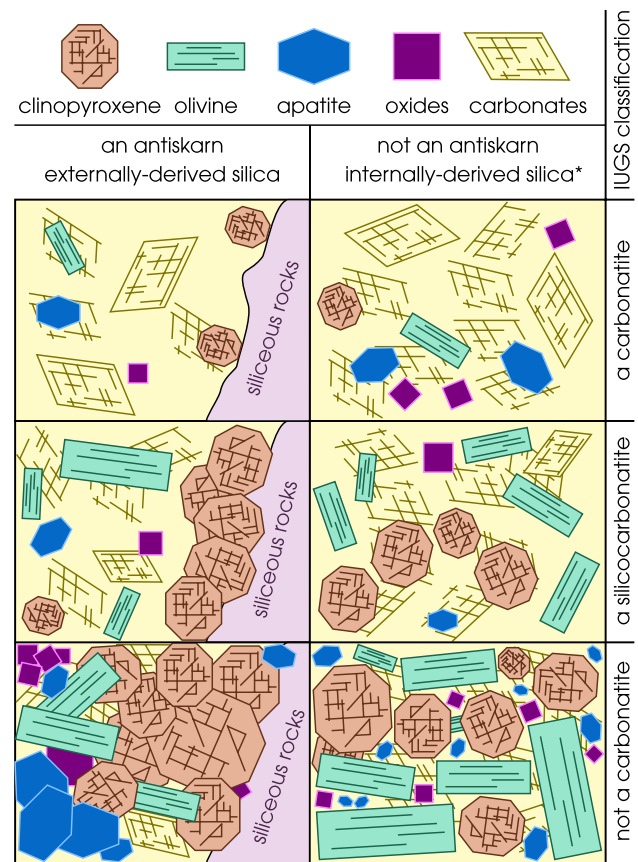

Fig. 1 A graphical representation of the relationships between antiskarns and silicocarbonatites. Note that "not a carbonatite" is defined according to the IUGS (Le Maitre et al. 2002). The recent redefinition of a carbonatite as any carbonate-containing rock that crystallised from a carbonatite melt regardless of carbonate mineral contents (Yaxley et al. 2022) would include these rocks in the "carbonatite" definition. Whether any substantial amount of internally-derived silica (marked by *) actually exists in carbonatites is questionable, see text for discussion

the silicate minerals formed concurrently with the carbonatitic magmatic activity. Rocks in which later hydrothermal fluids introduced silica, often in the form of quartz, are not considered here (e.g., the silicified carbonatites of Viladkar 2019; Zhang et al. 2022).

Experimental studies of antiskarn formation are limited by a narrow range of pressure (P) and temperature (T) conditions, and complicated chemical systems (Anenburg and Mavrogenes 2018; Vasyukova et al. 2023). Additionally, due to the challenging experimental design required to control oxygen fugacity (fO_2), the behaviour of ferric and ferrous Fe remains unknown. As minerals rich in Fe^{2+} and Fe^{3+} occur in carbonatite and antiskarn systems—appearing in minerals such as magnetite, ankerite, amphibole, and aegirine— understanding the fate of Fe during carbonatite metasomatism is a crucial aspect of antiskarn reactions, with potential

implications for other redox sensitive elements such as sulfur and carbon.

Here we present a computational thermodynamic study of phase relations in silica $\pm$ alumina-contaminated non-sodic, sodic, and potassic carbonatite systems. We examine the reactions and overall chemical and mineralogical trends that occur during introduction of SiO_2 to a solid assemblage characteristic of carbonatites. Finally, we expand on the new mechanism introduced by Vasyukova and Williams-Jones (2022) to explain some chemical and mineralogical characteristics observed in natural carbonatite complexes, such as the presence of abundant silicate minerals inside calcite carbonatites, and the ubiquitous association of carbonatites and pyroxenites or glimmerites (biotite-rich rocks), particularly when hosted by silica-rich wall rocks.

Thermodynamic modelling

We model solid–solid–fluid equilibrium during silica contamination of a carbonatite system. Due to lack of experimental data, there are no suitable activity-composition models for carbonatite melts, preventing a fully quantitative model (the models of Massuyeau et al. 2015 and Zhao et al. 2022 are mostly relevant for mantle pressures and do not cover the compositional range required here). However, it is a solid assemblage that is preserved in the geological record, and any silicate contamination of a carbonatite system is invariably recorded in the resulting minerals. Modelling of the solid–solid equilibria is also appropriate at high degrees of crystallisation and contamination in which the system transitions from melt-buffered to mineral-buffered. Thus, the modelled solid–solid and solid–fluid interactions provide useful semi-quantitative compositional trends that may be compared and contrasted with those in natural carbonatite systems. We emphasise that we are not modelling any real system with a constrained liquid line of descent or reaction path, but rather looking for

compositional variations in solid assemblages and associated C–O–H fluids. The systems considered here are initially simplified, but gradually build up to a comprehensive Na_2O–CaO–K_2O–FeO–MgO–Al_2O_3–SiO_2–H_2O–O_2–CO_2 system (see Table 1, and Fig. 2).

Equilibrium phase diagrams were calculated using the 2/12/2023 version of Perple_X 7.1.5 (Connolly 2009), thermodynamic database DS-62 (Holland and Powell 2011), and the following activity-composition models: oCcM(EF) (calcite–magnesite–siderite and dolomite–ankerite solid solutions, Franzolin et al. 2011), Omph(GHP) (clinopyroxene, Green et al. 2007), cAmph(G) (amphibole, Green et al. 2016), Pl(I1,HP) (ternary feldspar, Holland and Powell 2003), Neph(FB) (nepheline–kalsilite solid solution, Ferry and Blencoe 1978), Bi(W) (mafic micas, White et al. 2014), Sp_II(WPC) (magnetite and spinel, White et al. 2002), and O(HP) (forsterite and fayalite olivine, Holland and Powell 1998). The "naph" phase (Na-phlogopite) was excluded due to its persistent stability in Na_2O-bearing models at low levels (always below ~3.5%, often much lower), lack of Na in the Bi(W) model that could incorporate it, and negligible Na contents in natural micas from carbonatites and related rocks. Thus, this exclusion does not significantly impact the predicted phase equilibria. The CO_2 and H_2O components were transformed into elemental carbon and hydrogen with the excess oxygen added to the O_2 component, to permit the use of a generic hybrid molecular fluid equation-of-state solution model (GFSM) via the "GFSM T" keyword and "COH-Fluid" activity-composition model (Connolly 1995). Bulk compositions used in modelling are given in Table 1. Phase diagrams are calculated over a temperature range of 500–800 °C. Pressure effects at upper crustal conditions (100 to 500 MPa) are minimal and a mean value of 300 MPa is used as the sectioning pressure. Grid resolution was increased from the default by using "x_nodes 50 200" and "y_nodes 50 200" keyword options.

In low temperature metamorphic rocks (e.g. blueschist), differences in the space-group symmetry between ordered

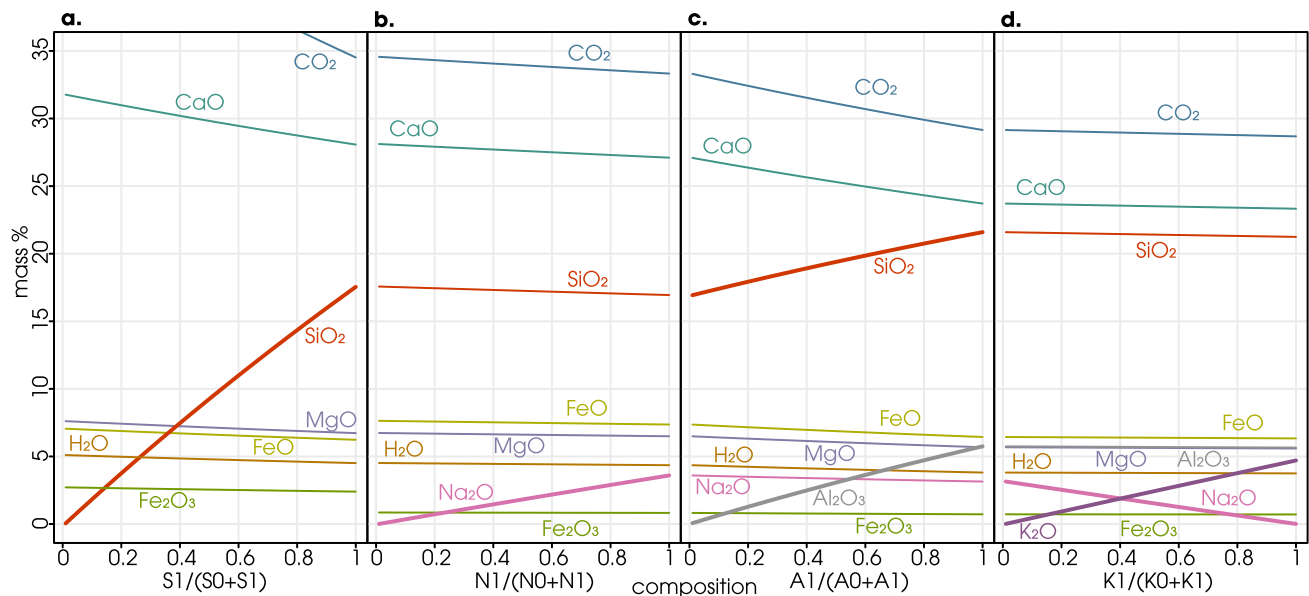|		S0	S1	N0	N1	A0	A1	K0	K1
Table 1 Absolute molar compositions used in Perple_X modelling	Na_2O	0	0	0.001	0.36	0.36	0.36	0.36	0.001
	CaO	3	3	3	3	3	3	3	3
	K_2O	0	0	0	0	0	0	0.001	0.36
	FeO	0.7	0.7	0.7	0.7	0.7	0.7	0.7	0.7
	MgO	1	1	1	1	1	1	1	1
	Al_2O_3	0.0005	0.0005	0.0005	0.0005	0.004	0.4	0.4	0.4
	SiO_2	0.004	1.75	1.75	1.75	1.75	2.55	2.55	2.55
	H_2O	0.75	0.75	0.75	0.75	0.75	0.75	0.75	0.75
	O_2	0.045	0.045	0.016	0.016	0.016	0.016	0.016	0.016
	CO_2	5.5	4.7	4.7	4.7	4.7	4.7	4.7	4.7

Fig. 2 The variation in oxide component relative proportions as the model compositions progress from **a** S0 to S1, **b** N0 to N1, **c** A0 to A1, and **d** K0 to K1. Changing components are marked with a bold line

disordered C2/*c* Ca pyroxene and P2/*n* Ca–Na omphacite results in two compositional regions of immiscibility between (1) Ca pyroxene and Ca–Na omphacite and (2) jadeite and Ca–Na omphacite (e.g., Matsumoto and Banno 1970; Tsujimori 2005). In contrast, both Ca pyroxene and aegirine are in the C2/*c* space group and full miscibility is expected. The Omph(GHP) model incorrectly predicts two-pyroxene assemblages for high-Fe^{3+}–low-Al Ca–Na pyroxenes at low temperatures in our phase diagrams. Here we allow immiscibility, but take the averaged abundance and composition of the two pyroxene phases where erroneous two-pyroxene immiscibility occurs.

Silica activity was calculated by modelling a SiO_2-only system using identical gridding parameters, leading to a pure assemblage of quartz across the entire *T*–*X* range. Chemical potential was extracted from the pure quartz and the carbonatite models, and then used in the following equation to derive silica activity:

$$aSiO_2 = \exp\left(\frac{\mu_{SiO_2}^{model} - \mu_{SiO_2}^{quartz}}{RT} \right).$$

Oxygen fugacity (fO_2) was expressed relative to the fayalite–magnetite–quartz (FMQ) buffer calculated by modelling an assemblage of fayalite, magnetite, and quartz endmembers. Chemical potential of O_2 was extracted from the FMQ assemblage and the carbonatite model, and used in the following equation to compute oxygen fugacity (Anenburg and O'Neill 2019):

$$fO_2 = \frac{\mu_{O_2}^{model} - \mu_{O_2}^{FMQ}}{\ln 10 RT}.$$

The exclusion of melt is not detrimental to this model, because at the relatively low temperatures considered here, a carbonatite melt is likely to be multiply saturated with many minerals. The solid phase compositions are constrained by their mutual equilibrium in a system with low degrees of freedom such that any melt compositions are likewise determined and have little influence on the solid phases. In other words, the solid assemblage buffers the melt composition. Because carbonatite melts are not modelled here, equilibrium states between components derived from the presumed melt (e.g. Na_2O and K_2O) and components derived from contaminating silicate rocks (e.g. SiO_2 and Al_2O_3) require a different approach. *X*0 compositions such as N0 or K0 reflect a scenario where the chemical component (Na_2O and K_2O in our example, respectively) is wholly soluble in the melt and not available for silicate phase formation. Increasing their amounts in our models mimics a process in which those components are pulled out of the melt, simulating the decrease of their solubility during silica contamination. By comparing these series of equilibrium states with natural rocks, we can test our assumptions on melt behaviour despite a melt phase not being included in the models. That the mineral compositions and assemblages parallel those found in nature (as will be evident below) is validation that the exclusion of carbonatite melt does not significantly influence our results.

In our modelling, we use mostly constant C, H, and O contents. This has two major effects. First, it constrains the stability fields of hydrous or carbonated phases to fixed positions in our phase diagrams. However, we use a wide composition range such that all assemblages of interest, as observed in natural rocks, are considered in the modelling. Allowing for variable C–O–H fluid bulk compositions—for example by buffering fugacities—will shift some phase boundaries on the diagrams at the cost of increased complexity. Second, it allows us to examine how chemical potentials of fluid components vary based on the solid mineral assemblage, and decouple them from any potential open system behaviour of the fluid. For example, we do not model decarbonation reactions via changing CO_2 contents. Instead, we model how introduction of silica forces decarbonation for a given bulk composition. Our specified C–O–H components result in CO_2-rich compositions, as is often observed in natural carbonatites. Pure aqueous synmagmatic fluids are highly atypical.
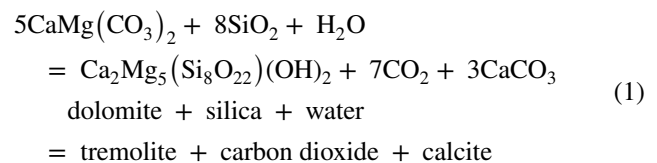
Results

Pseudosections and modelling results for 300 MPa are shown in Figs. 3, 4, 5 and 6, whereby each panel shows the variability of a single parameter in $T–X$ space. All "moles of…" panels show absolute molar abundance, not percentage. Details of all other parameters are given in Table 2. Figures 3, 4, 5 and 6 only show the key results of our modelling. We strongly encourage this paper is read alongside the Supplementary Figures, which contain the complete set of phase abundances and compositions, for 300 MPa as well as 100 and 500 MPa, along with pseudosections for all pressures, and derivation notes for calculated parameters.

The system $CaO–FeO–MgO–SiO_2–H_2O–O_2–CO_2$ (S0–S1)

For the first compositions (S0–S1), we consider the addition of SiO_2 to the solid assemblage of calcite, dolomite, and magnetite (Fig. 3). Carbonatite melts are often saturated with these three minerals for a portion of their crustal evolution duration and the solid calcite–dolomite–magnetite assemblage approximates magmatic carbonatite systems, particularly below ~900 °C when silica is mostly insoluble (Yaxley et al. 2022). Silica is added into the base carbonatite composition (S0), up to the amount shown as S1 in Table 1, and Fig. 2a. Carbon dioxide contents were initially set to be slightly in excess, such that all metal oxides have associated carbonate anions, if stable. Carbon dioxide contents are reduced towards S1 due to some metal cations sequestered in silicate minerals, releasing additional CO_2 and negating the

need for a large excess. A negligible but nonzero amount of Al_2O_3 was introduced to correctly stabilise the Omph(GHP) model.

The observed assemblages are, as a first approximation, similar to those observed in metamorphosed silica-bearing carbonate rocks (Moore and Kerrick 1976; Tracy and Frost 1991), and metasomatism at the contact between siliceous intrusions and carbonate rocks (i.e. skarns, Cook and Bowman 2000). At least for this simplified system (CFM-SHO + CO_2), the equilibrium and reactions are essentially the same in both skarns and antiskarns. The difference lies in the formation mechanism and geological setting. For example, at low temperatures (< 590 °C), addition of silica leads to formation of Ca-amphibole and calcite at the expense of dolomite (Fig. 3a, Supp. Figures 1–6), approximated by the following simplified reaction:

$$5CaMg(CO_3)_2 + 8SiO_2 + H_2O$$
$$= Ca_2Mg_5(Si_8O_{22})(OH)_2 + 7CO_2 + 3CaCO_3$$
$$\text{dolomite} + \text{silica} + \text{water} \qquad (1)$$
$$= \text{tremolite} + \text{carbon dioxide} + \text{calcite}$$

The partitioning of Mg from carbonate to silicate phases leads to enrichment of the Fe-endmembers ankerite in dolomite and siderite in calcite (Fig. 3f, Supp. Figures 1–6), which themselves break down at higher X_{S1} leading to a Fe-richer amphibole at high SiO_2 contents (Fig. 3, Supp. Figures 1–6). Details and discussions of further phase relations and reactions occurring between forsterite, diopside, tremolite, calcite, and dolomite in $CO_2–H_2O$-bearing systems are available in most metamorphic petrology textbooks.

At higher temperatures (> 600 °C) clinopyroxene and olivine predominate, with their proportions a function of the amount of added silica. Initially, dolomite is destabilised in favour of calcite and olivine until about $X_{S1} = 0.3$ (Fig. 3a, c, Supp. Figures 1–6), followed by assemblages with calcite and diopside at higher X_{S1}. The relevant reactions in the natural system are similar to Reaction (1), but without H_2O as a reactant and with olivine and diopside instead of amphibole as a product.

For most of the modelled space, magnetite contains a minor magnesioferrite component, except at high temperature and low X_{S1} in which magnetite becomes substantially magnesian (Fig. 3e). This is reflected in fO_2 which likewise attains lower values at these conditions, and an increase in reduced fluid species (Fig. 3b, Supp. Figure 1–6). Interestingly, fO_2 shifts substantially (~3 log units) without any change in the bulk O_2 contents, but instead by (1) a redistribution of Fe^{3+} between different minerals as a function of temperature and the concentration of a
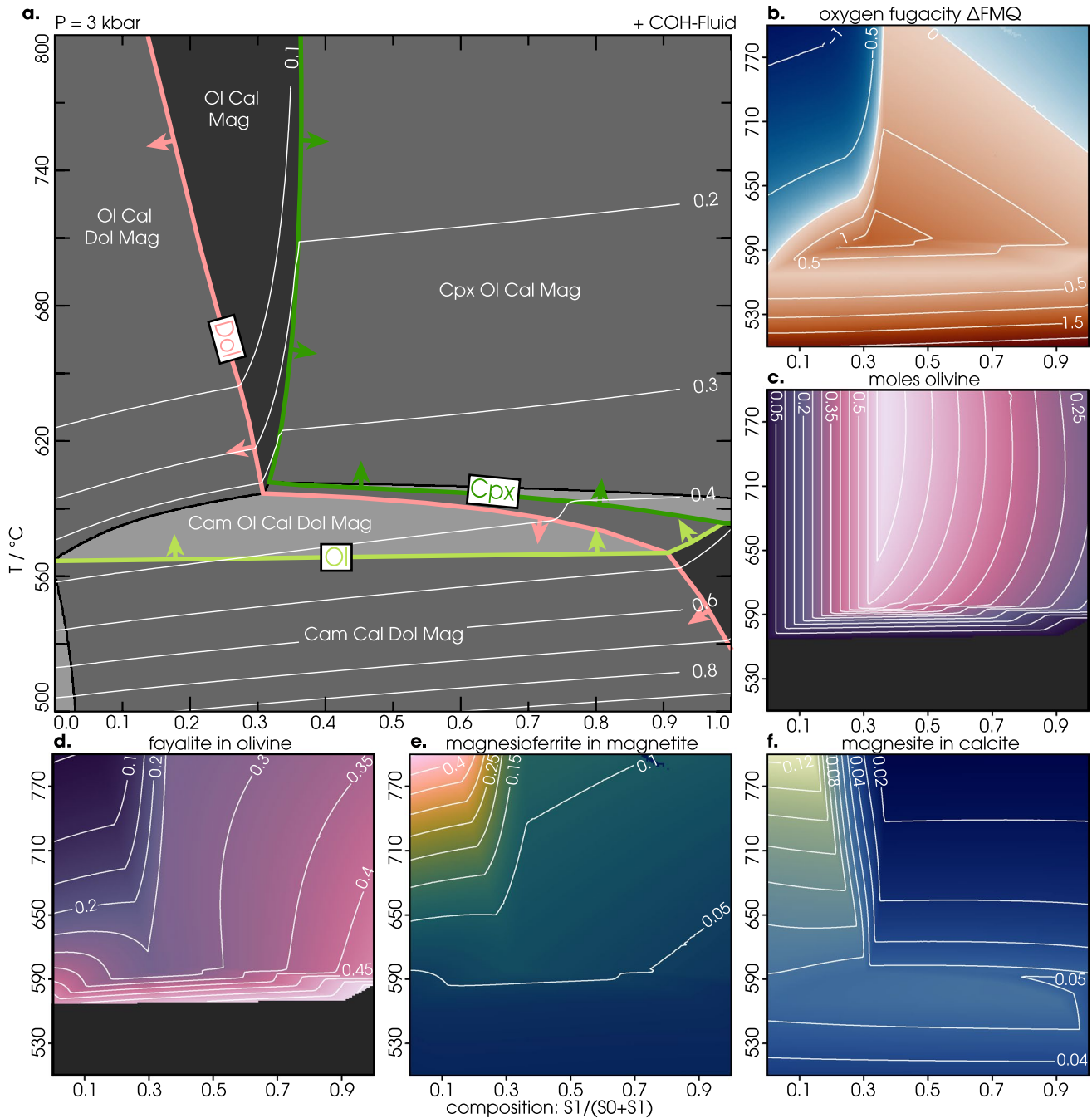
Fig. 3 **a** Pseudosection for the system S0–S1 with the boundaries for dolomite (pink), olivine (light green), and clinopyroxene (dark green) bearing fields highlighted. Silica activity is also contoured (white lines). Side panels show additional contours of **b** fO_2, **c** moles of olivine, **d** fayalite component in olivine, **e** magnesioferrite component in magnetite, and **f** magnesite component in calcite

non-redox sensitive component (SiO_2), and (2) differences in the T–fO_2 slopes between the modelled assemblage and FMQ at constant compositions. Silica activity is similarly strongly dependent on temperature, with higher values at lower temperatures (Fig. 3a). An extension of the model to lower temperatures will result in silica forming quartz instead of ferromagnesian silicate minerals (as observed to form via low temperature and late stage fluids in carbonatites, Zhang et al. 2022), but this process is beyond the scope of this manuscript.
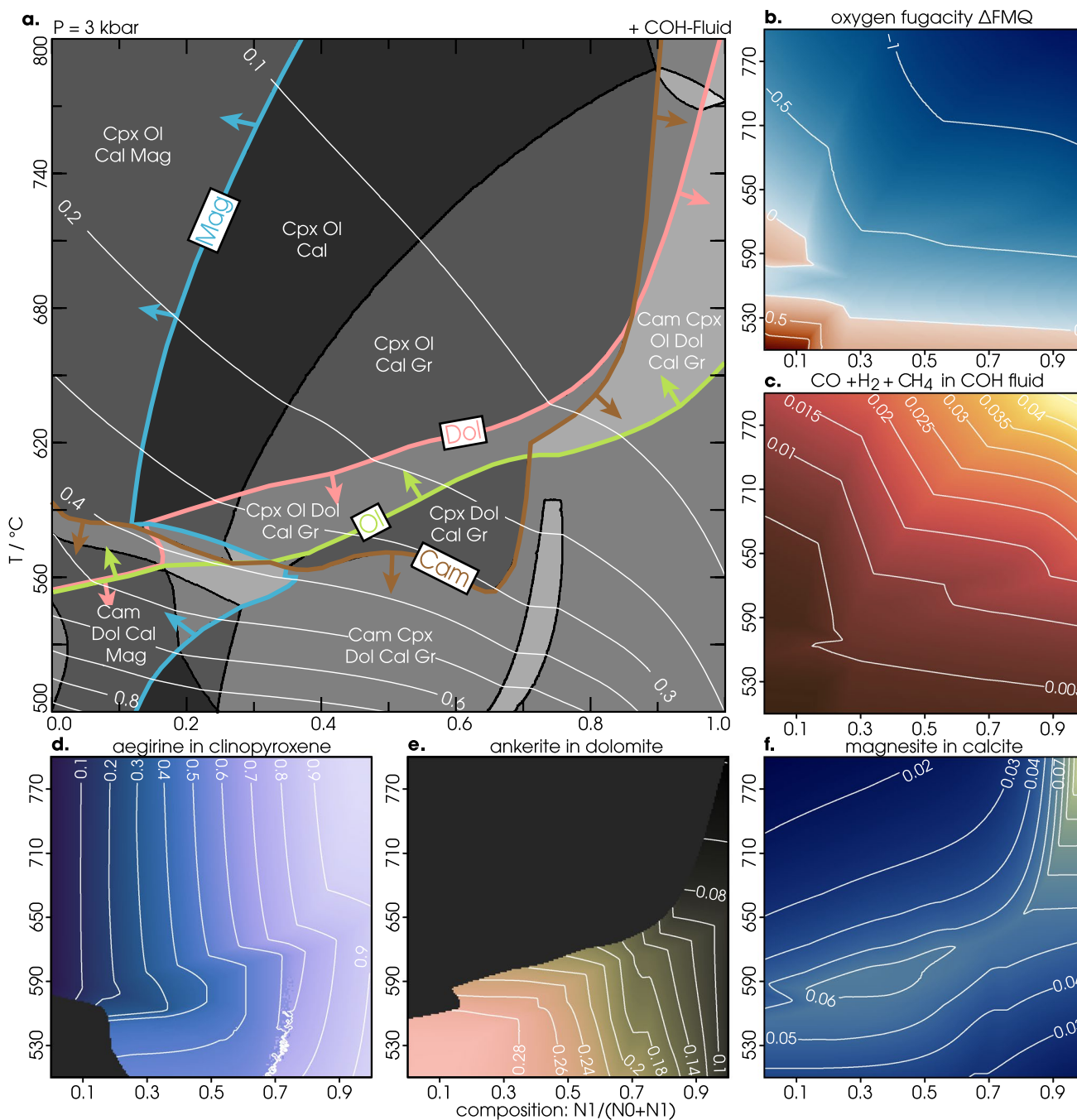
Fig. 4 **a** Pseudosection for the system N0–N1 with the boundaries for dolomite (pink), olivine (light green), magnetite (blue), and clinoamphibole (brown) bearing fields highlighted. Silica activity is also contoured (white lines). Side panels show additional contours of **b** fO_2, **c** combined mole fraction of reduced fluid species, **d** aegirine component in clinopyroxene, **e** ankerite component in dolomite, and **f** magnesite component in calcite

The system $Na_2O–CaO–FeO–MgO–SiO_2–H_2O–O_2–CO_2$ (N0–N1)

Carbonatite melts are often highly sodic. Sodium contents are known to increase in the later stages of carbonatite evolution (Chayka et al. 2021; Mollé et al. 2022; Weidendorfer et al. 2017; Yaxley et al. 2022). However, no Na-carbonate or oxide phases exist in the Holland and Powell (2011) thermodynamic database. As a result, the addition of Na_2O as a component requires additional silica to form
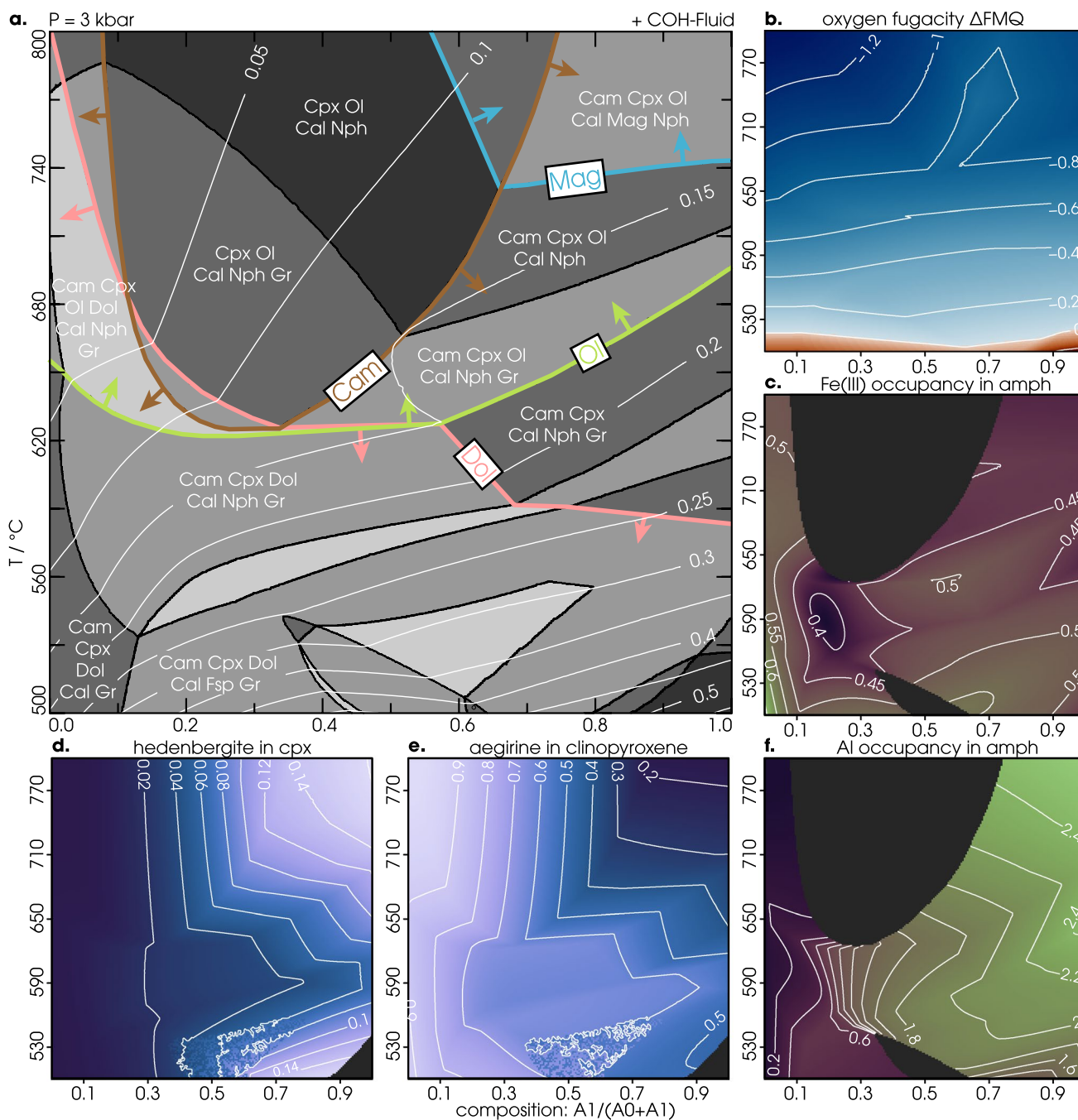
Fig. 5 **a** Pseudosection for the system A0–A1 with the boundaries for dolomite (pink), olivine (light green), magnetite (blue), and clinoamphibole (brown) bearing fields highlighted. Silica activity is also contoured (white lines). Side panels show additional contours of **b** fO_2, **c** Fe^{3+} in clinoamphibole, **d** hedenbergite component in clinopyroxene, **e** aegirine component in clinopyroxene, and **f** Al occupancy in clinoamphibole

Na-silicates, which are listed in the thermodynamic database. Thus, practical constraints only allow exploring the compositional space between Na_2O-free and Na_2O-rich silica-bearing carbonatite endmembers. We therefore adjust the S1 composition to create N0: an initial carbonatite that already contains silica, from which we derive N1 with elevated contents of Na_2O (Table 1, Fig. 2b), with a maximum content limited by SiO_2. The amount of oxygen is lowered to better demonstrate the reduction of CO_2 (see below). Given that total Fe remains the same, this has the additional effect of increasing Fe^{2+}/Fe^{3+}, similar to differentiation in
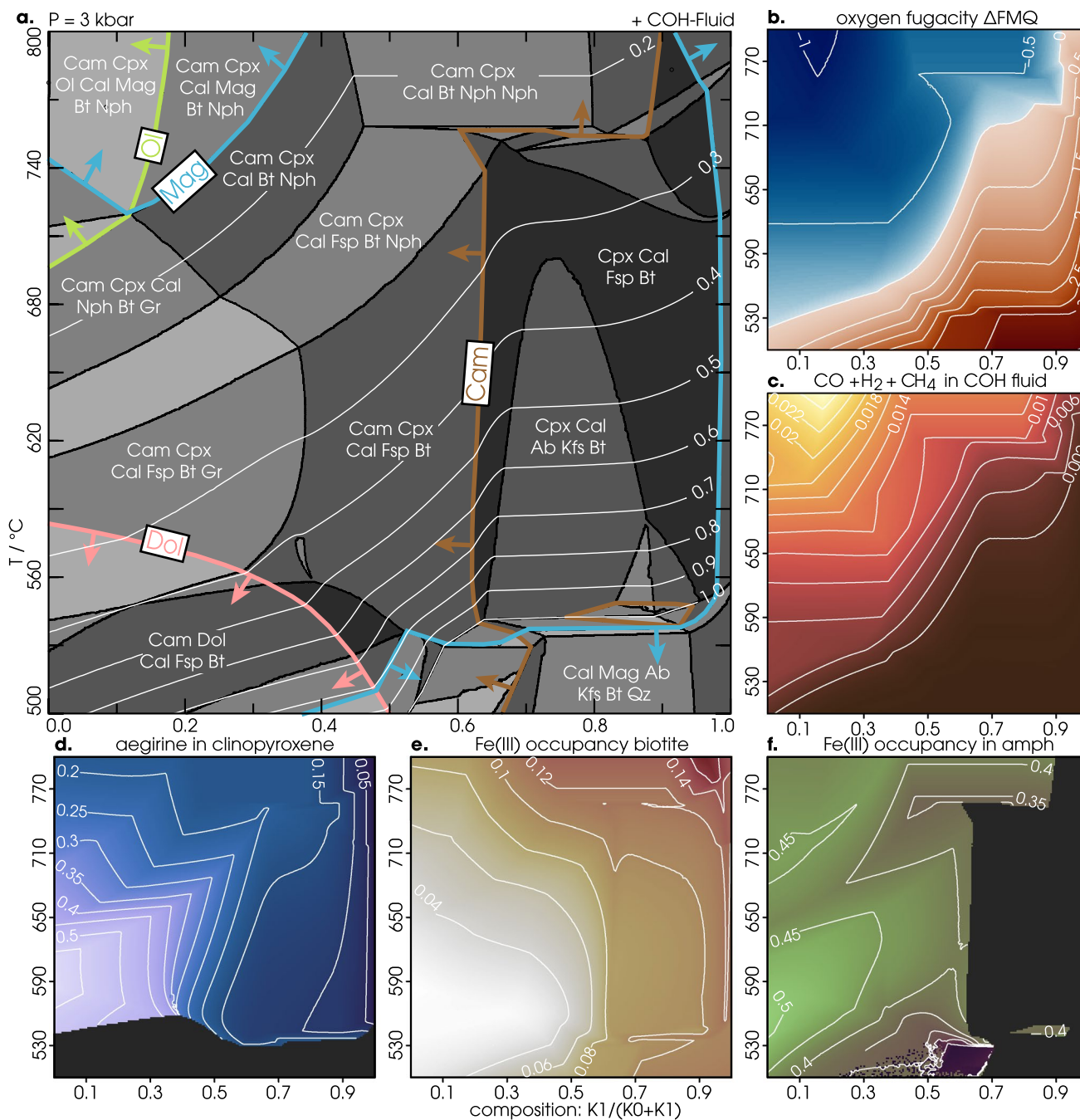
Fig. 6 a Pseudosection for the system K0–K1 with the boundaries for dolomite (pink), olivine (light green), magnetite (blue), and clinoamphibole (brown) bearing fields highlighted. Silica activity is also contoured (white lines). Side panels show additional contours of **b** fO_2, **c** combined moles of reduced fluid species, **d** aegirine component in clinopyroxene, **e** Fe^{3+} occupancy in biotite, and **f** Fe^{3+} occupancy in clinoamphibole

natural carbonatite systems because magnetite is typically an early crystallising mineral (Anenburg et al. 2021).

The principal host phase for Na is the aegirine endmember in clinopyroxene (Fig. 4). Throughout most of the modelled *T–X* space, clinopyroxene abundance remains roughly constant, but aegiri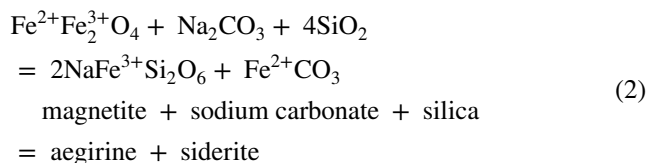ne contents increase almost linearly with the increase of Na_2O, replacing the hedenbergite component (Fig. 4d, Supp. Figures 7–12). At $X_{N1} < 0.2$–0.3, the ferric component of magnetite is consumed to form the aegirine component in clinopyroxene (Supp. Figures 7–12), with the ferrous component mostly partitioned to calcite as the

Table 2 Compositional parameters

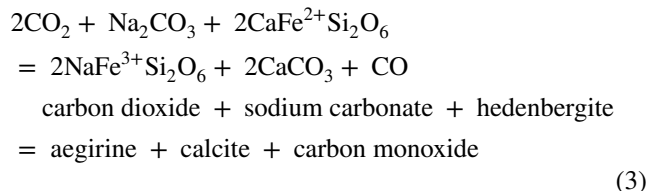| Phase (abbreviation)	Compositional parameter	Component or endmember fraction formula
Calcite (Cal)	Magnesite	$\dfrac{MgO}{CaO+FeO+MgO}$
	Siderite	$\dfrac{FeO}{CaO+FeO+MgO}$
Dolomite (Dol)	Ankerite	$\dfrac{FeO}{FeO+MgO}$
Olivine (Ol)	Fayalite	$\dfrac{fa}{fa+fo}$
Magnetite (Mag)	Magnesioferrite	$\dfrac{-herc}{mt+sp+herc}$
	Al occupancy	$\dfrac{sp+herc}{mt+sp+herc}$
Clinopyroxene (Cpx)	Hedenbergite	$\dfrac{hed+0.5cfm}{di+jd+acm+hed+om+cfm+jac}$
	Aegirine	$\dfrac{0.5jd+acm+0.5om+0.5jac}{di+jd+acm+hed+om+cfm+jac}$
	Al occupancy	$\dfrac{jd+0.5om+0.5jac}{di+jd+acm+hed+om+cfm+jac}$
Clinoamphibole (Cam)	Fe(II) occupancy	$\dfrac{7grun+4a+5b}{7(mrbG+gl+ts+parg+kprg+cumm+grun+tr+a+b)}$
	Fe(III) occupancy	$\dfrac{mrbG}{mrbG+gl+ts+parg+kprg+cumm+grun+tr+a+b}$
	Na occupancy	$\dfrac{2mrbG+2gl+parg}{3(mrbG+gl+ts+parg+kprg+cumm+grun+tr+a+b)}$
	Al occupancy	$2_{Al_2O_3}$
	K-pargasite	$\dfrac{kprg}{mrbG+gl+ts+parg+kprg+cumm+grun+tr+a+b}$
Nepheline (Neph)	Kalsilite	$\dfrac{kls}{ne+kls}$
Feldspar (Fsp)	K	$\dfrac{san}{san+abh+an}$
	Ca	$\dfrac{an}{san+abh+an}$
Biotite (Bt)	Fe(II) occupancy	$\dfrac{2ann+1obi}{3(fbi+east+ann+phl+obi)}$
	Fe(III) occupancy	$\dfrac{fbi}{fbi+east+ann+phl+obi}$
COH-Fluid	$CO+H_2+CH_4$	$\dfrac{CH_4+H_2+CO}{CO_2+CH_4+H_2+CO+H_2O}$
	H_2O	$\dfrac{H_2O}{CO_2+CH_4+H_2+CO+H_2O}$

See Supplementary Materials along with the Perple_X solution_model.dat for more details. Abbreviations are after Warr (2021).

siderite component. In a natural system, such a process would take the form of the reaction:

$$Fe^{2+}Fe_2^{3+}O_4 + Na_2CO_3 + 4SiO_2$$
$$= 2NaFe^{3+}Si_2O_6 + Fe^{2+}CO_3$$
$$\text{magnetite } + \text{ sodium carbonate } + \text{ silica} \qquad (2)$$
$$= \text{aegirine } + \text{ siderite}$$

The sequestration of silica in aegirine leads to a substantial drop in silica activity (Fig. 4a), stabilising dolomite to higher temperatures at the expense of olivine and the diopside component of clinopyroxene (Supp. Figure 7–12). Dolomite and clinopyroxene were mutually exclusive in the Na-free model above, but here they are stable together for all but the Na-poorest compositions. Towards $X_{N1} = 1$, aegirine consumes most SiO_2, and silica activity becomes sufficiently low that olivine destabilises (Supp. Figure 7–12), with the Mg partitioning into calcite as the magnesite component (Fig. 4f).

At $X_{N1} > 0.2$–0.3 magnetite is exhausted (Fig. 4a). Nonetheless, the addition of Na_2O must stabilise aegirine. The fixed amount of excess O_2 between N0 and N1 requires that Fe^{3+} is produced by oxidation of Fe^{2+} in FeO by reducing C in CO_2 to CO, H in H_2O to H_2, or both to CH_4 (Fig. 4c). All Fe^{2+}-bearing phases show a decrease in their Fe^{2+} contents with increasing X_{N1} (e.g. Fig. 4e, Supp. Figures 7–12). Such a process may occur in natural systems through the reaction of Na_2CO_3 with hedenbergite (here using CO for simplicity):

$$2CO_2 + Na_2CO_3 + 2CaFe^{2+}Si_2O_6$$
$$= 2NaFe^{3+}Si_2O_6 + 2CaCO_3 + CO$$
$$\text{carbon dioxide } + \text{ sodium carbonate } + \text{ hedenbergite}$$
$$= \text{aegirine } + \text{ calcite } + \text{ carbon monoxide}$$
$$(3)$$

In our models, amphibole which is stable below 580 °C, becomes Na–Fe^{3+}-dominant at X_{N1} close to 1 (Supp. Figures 7–12), thus a reaction comparable to Reaction (3) may occur with amphibole as a product instead of aegirine.

The full consumption of magnetite marks a significant change in the fO_2 of the predicted phase assemblages

(Fig. 4b). At higher X_{N1} the slopes are sub-horizontal, indicating that the aegirine-forming reactions serve as an fO_2 buffer, with gradual increase of reduced fluid species. Some reduced carbon is also predicted as solid graphite, particularly at lower temperatures (Supp. Figures 7–12).

The system Na_2O–CaO–FeO–MgO–Al_2O_3–SiO_2–H_2O–O_2–CO_2 (A0–A1)

Silica contamination is rarely accomplished on its own. Often, the silica is sourced from Al-bearing minerals in the wall rocks, introducing an Al_2O_3 source. Compositionally, A0 is identical to N1, and towards A1 there is an increase of both Al and Si on a 1:1 molar basis as to not dilute the previous introduction of SiO_2 (Table 1). The complete variation in relative oxide proportions from A0 to A1 is shown in Fig. 2c.

Elevated Al_2O_3 contents strongly expand amphibole stability fields (Fig. 5). As expected, the combined introduction of Al_2O_3 and SiO_2 primarily stabilises nepheline at temperatures greater than about 600 °C and albite at lower temperatures (Fig. 5, Supp. Figures 13–18). Their coexistence in natural rocks will buffer $aSiO_2$ close to 0.23 via the reaction:

$$NaAlSiO_4 + 2SiO_2 = NaAlSi_3O_8$$
$$nepheline + silica = albite \tag{4}$$

Both minerals require Na, which is primarily sourced from aegirine. This has the knock-on effect of reversing the sodium introduction model (N0–N1, Fig. 4), leading to (1) a modest increase of fO_2 (Fig. 5b), (2) increase of silica activity (Fig. 5a), (3) increase of the hedenbergite and diopside components in clinopyroxene (Fig. 5d, Supp. Figure 13–18), (4) increase of Fe^{2+} proportions in most phases (Fig. 5c, d), and (5) modest increase of oxidised species in the fluid (Supp. Figure 13–18). In particular, magnetite is stable only above 730 °C at > 0.5 X_{A1}, whereas previously magnetite was stable only at low silica contamination (Figs. 3, 5). However, these reversals are not completed due to Al-enhanced amphibole stability (Fig. 5f): the predicted amphibole is highly sodic, retaining Fe^{3+} as the arfvedsonite, riebeckite and nybøite components (Fig. 5c, Supp. Figure 13–18). As a result, Fe-oxidation and C-reduction driven by O_2 partitioning also stabilises graphite and reduced fluid species in the A0–A1 model (Fig. 5a, Supp. Figure 13–18). Dolomite is again consumed to form olivine and calcite according to Reaction (2) (Supp. Figure 13–18). Ultimately, the partitioning of Fe^{3+} between silicate phases, amphibole and clinopyroxene, as opposed to a silicate and oxide, results in only moderate changes in fO_2 with varying degree of contamination (Fig. 5b).

The system Na_2O–CaO–K_2O–FeO–MgO–Al_2O_3–SiO_2–H_2O–O_2–CO_2 (K0–K1)

Finally, to examine the contrasting effect of K relative to Na, composition A1 is replicated as K0 and towards K1, Na_2O is gradually replaced by K_2O on an atom-by-atom basis (Table 1, Fig. 2d). This stabilises micas and permits the introduction of K into minerals with a Na–K solid solution (amphibole, feldspar, nepheline).

The most obvious result of adding K is biotite formation at the expense of other magnesian and aluminous phases (Fig. 6, Supp. Figures 19–27). Olivine is not predicted throughout much of the modelled space (Fig. 6a). Dolomite is also destabilised at higher K_2O contents (particularly at $X_{K1} > 0.4$, Fig. 6a, Supp. Figure 13–18). Lower feldspar and nepheline abundances occur as alkalis and Al_2O_3 are transferred to biotite (Supp. Figure 13–18). These phases remain entirely sodic until a dramatic switch to potassic compositions is predicted over a short interval of roughly 0.2 X_{K1} units at $X_{K1} > 0.5$ (Supp. Figure 13–18). The phase boundary between K-feldspar and kalsilite occurs at a higher temperature compared to the albite–nepheline boundary. These two minerals also buffer $aSiO_2$ (Fig. 6a) via:

$$KAlSiO_4 + 2SiO_2 = KAlSi_3O_8$$
$$kalsilite + silica = K\text{-}feldspar \tag{5}$$
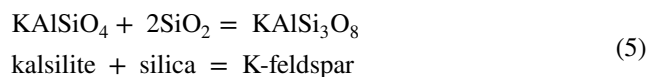
Aegirine contents of clinopyroxene drop to zero towards $X_{K1} = 1$ (Fig. 6d), where some Fe^{3+} is partitioned into magnetite (Supp. Figure 13–18). This is accompanied by a drastic increase in silica activity and fO_2 (Fig. 6a, b), and destabilisation of graphite and reduced fluid species (Fig. 6c). Despite the elevated fO_2 conditions, in some cases higher than those prevailing in the S0–S1 model, magnetite is only sparsely stable (Fig. 3b, 6b). Instead, Fe^{3+} is sequestered in the tetraferriphlogopite component in biotite (Fig. 6e) and sodic amphibole (Fig. 6f). However, fO_2 greatly increases because buffering reactions depend on the composition, not the amount, of reactants and products, and the predicted oxide is nearly pure magnetite (Supp. Figure 13–18).

We encounter the alkali feldspar solvus in our modelling (Fig. 6a). At lower pressures, this solvus is truncated by the limited feldspar stability relative to nepheline and kalsilite (Fig. 7). With increasing pressure, the feldspar–nepheline boundary rises in temperature at a higher rate than the solvus. At 3 kbar there is a small temperature gap of about 40 °C in which a single intermediate feldspar is stable above the solvus, and this gap increases with pressure (Fig. 7). This feldspar–nepheline relationship indicates that a single feldspar with perthite exsolution is expected at high pressures whereas two feldspars are expected at lower pressures. This behaviour is opposite to the classic one-or-two feldspar granites, in which two
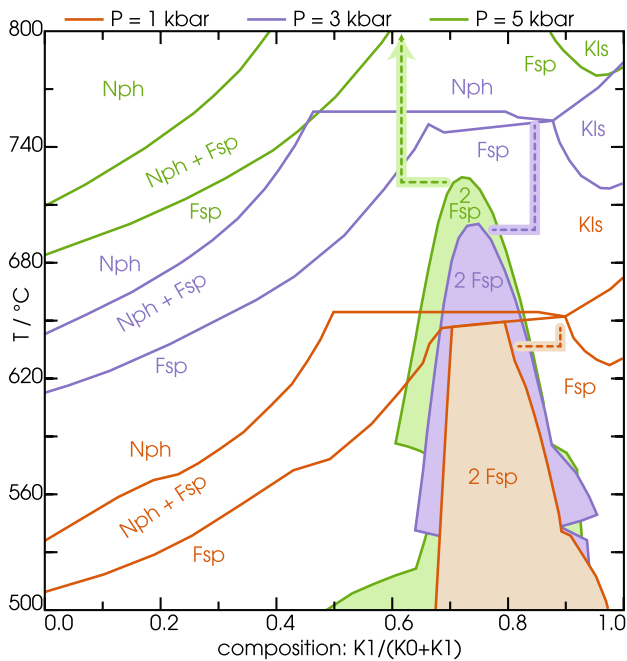
Fig. 7 Simplified pseudosection showing stability fields of feldspars, nepheline, and kalsilite at 1 (red), 3 (purple), and 5 kbar (green). Shaded fields indicate two feldspar fields. Thick dashed lines indicate the temperature gap within the one feldspar field between top of the feldspar solvus and nepheline or kalsilite stability fields

feldspars are expected at higher pressures (Bowen and Tuttle 1950; Morse 1970).

Discussion

Our modelling results strongly depend on the starting compositions used as model inputs. Furthermore, we chose a single compositional point of a previous modelling step as the starting point for the next, out of essentially infinite possibilities. As a result, we mostly avoid referring to specific or quantitative compositions. Temperature ranges of phase stabilities and reactions shift with pressure, and the choice of 3 kbar is somewhat arbitrary. Models calculated at 1 and 5 kbar are available in the Supplementary Materials and allow examination of the pressure effect on phase equilibria. Such an approach allows us to test the sensitivity of the system and predict the relative effects of silica contamination of a carbonatite melt. Here we extrapolate our predictions to trends found in natural rocks.

Note that the models represent possible equilibrium states, and do not imply a process or a path. That is, a progression from low $X0$ to high $X1$ on any model is not meant to replicate a process occurring in nature. We are conducting sensitivity testing using a series of equilibrium states to see the possible effects of different bulk

compositions on the predicted mineral assemblages, their solid solution, and fluid compositions. Any natural petrological process will follow a non-linear segment that likely hops between compositional models, including (and likely) those which we have not modelled. We encourage readers to make use of the modelling files available in the Supplementary Materials to derive their own comparable models and explore additional compositions.

Silicocarbonatites—result of silica contamination?

The formation of silicocarbonatites has been much debated (Brady and Moore 2012; Chakhmouradian et al. 2008; Giebel et al. 2019; Viladkar 2019). The simplest offered explanation is that any silicate minerals found in such rocks are phenocrysts crystallising directly from the carbonatite melt (e.g. Moore et al. 2022; Prokopyev et al. 2021, and illustrated in the bottom right of Fig. 1). This hypothesis is challenged by the low solubility of SiO_2 in crustal carbonatites. For example, nepheline, biotite, and olivine are common minerals in silicocarbonatites. All three contain about 40 wt% SiO_2. A typical silicocarbonatite containing 25% of any of these minerals would then have 10 wt% SiO_2 in the bulk rock. Other common silicocarbonatite minerals such as clinopyroxenes or amphiboles would raise the bulk rock SiO_2 contents even higher, as their SiO_2 contents reach around 50 wt%. Experimental works on the composition of immiscible carbonatite–silicate melts at crustal pressures (< 1 GPa) show that SiO_2 contents rarely exceed 5 wt% in the carbonatite melt (Brooker and Kjarsgaard 2011; Kjarsgaard 1998; Kjarsgaard and Hamilton 1988; Kjarsgaard et al. 1995), and are negligible at temperatures below ~ 1000 °C (Anenburg and Guzmics 2023; Weidendorfer and Asimow 2022), although not without controversy (Berndt and Klemme 2023). At mantle pressures (≥ 2 GPa), SiO_2 contents can be higher, but only reach concentrations of < 10 wt% (Martin et al. 2013, 2012). If carbonatite rock compositions are taken to represent the melts from which they crystallised, this poses a paradox. The low silica solubilities mean that silicates in a silicocarbonatite cannot crystallise directly from the carbonatite melt. However, carbonatite rocks are in fact cumulates which do not represent the melt from which they crystallised (Veksler et al. 1998; Wei et al. 2020; Yaxley et al. 2022), and the modal mineral proportions can represent any minerals crystallising from the melt at the time. In that case, a silicocarbonatite might comprise a volume subset of an entire carbonatite intrusion which happened to capture crystallising silicates (e.g., Cooper and Reid 1998, and again consistent with the illustration in the bottom right of Fig. 1). However, this process, like direct phenocryst crystallisation, cannot result in silicocarbonatites

because solidifying carbonatite melts primarily crystallise calcite and dolomite, whereas silicates only consist of a minor part of any instantaneous cotectic assemblage crystallising at a given time. For example, Weidendorfer et al. (2017) show that a fractionating carbonatite melt will only form around 4% clinopyroxene compared to the amount of calcite formed. Likewise, experiments by Anenburg et al. (2020b) show that in their clinopyroxene-saturated carbonatite (i.e., the carbonatite melt has as much as SiO_2 as possible, cf. Barker 2001), the crystallising carbonatite leads to an assemblage dominated by calcite and about 5% olivine. The phase diagrams given by Lee and Wyllie (2000) similarly indicate that only a very small amount of clinopyroxene or olivine will crystallise together with calcite or dolomite. These studies make it apparent that silicocarbonatites cannot form by accumulation of silicate minerals from a crystallising carbonatite melt. Whilst we have no objection to some silicocarbonatites containing silicate antecrysts forming during the carbonatite melt ascent from a hot (~ 1200 °C) mantle (Moore et al. 2022; Stoppa et al. 2019), these systems represent a minority among silicocarbonatites in which silicate minerals are typically of a cooler crustal origin.

Here we suggest that silicocarbonatites form when carbonatite melts react with surrounding siliceous wall rocks and leach $SiO_2 \pm Al_2O_3$. The term often used in relation to silicate magmas is "assimilation". However, assimilation implies that solid components from the wall rock are dissolved and transported into the silicate melt, to remain in liquid solution. Here, the presence of the assimilated wall rock components in the carbonatite melt is merely ephemeral, as any additional SiO_2 is rapidly deposited into solid mineral phases. The leaching reaction triggers saturation of silicate minerals in the carbonatite melt due to their low solubility. Practically, the carbonatite melt functions as a flux-diffusion medium that transports SiO_2 from the wall rocks into crystallising minerals.

In nature, silicate minerals forming by silica contamination can misleadingly appear as phenocrysts. There is no requirement for the silicate minerals to form at the carbonatite–silicate reaction interface. For example, reaction experiments between liquid carbonatites and solid silicates by Anenburg and Mavrogenes (2018) resulted in olivine crystals that formed deep within the carbonatite section of the experimental capsule, and not in direct contact with the original silicate mineral assemblage. Hode Vuorinen and Skelton (2004) demonstrated that crystals which were originally present in wall rocks surrounding carbonatite dykes at Alnö (Sweden) were removed into the carbonatite during its intrusion. The crystals were then chemically modified such that they have the false appearance of primary phenocrysts when they were in fact xenocrysts. Particularly instructive is the case of the Caotan carbonatite, which contains

uncontaminated dolomite carbonatites in close proximity to silica-contaminated olivine calcite carbonatites (Wei et al. 2020). Both calcite and dolomite carbonatites contain roughly similar CaO and MgO contents, but the contaminated calcite carbonatite contains up to ~ 17 wt% SiO_2 (bringing it close to the formal silicocarbonatite 20 wt% SiO_2 threshold), whereas the uncontaminated dolomite carbonatite contains much lower SiO_2, between 0.3 wt% and 2.6 wt% (Wei et al. 2020).

Although we previously emphasised the low silica solubility in carbonatite melts, detailed work by Brooker and Kjarsgaard (2011) and Otto and Wyllie (1993) revealed that SiO_2 contents greater than 10 wt% are possible in cases of alkali-poor carbonatite melts. Although most carbonatite rocks are indeed alkali-poor, this is misleading as the melts from which these crystallised were alkali-rich. Evidence includes the ubiquitous occurrence of surrounding fenite aureoles, alkali-rich fluid and melt inclusions, and the composition of the silicate minerals themselves with potassic micas, and sodic clinopyroxenes and amphiboles (Yaxley et al. 2022).

Clinopyroxene compositions

Clinopyroxenes in carbonatites and related rocks often exhibit a compositional trend which starts with pure diopside compositions, followed by an increase in Fe which is distributed mostly as hedenbergite and marginally as aegirine. The trend concludes with a strong increase of the aegirine component at the expense of both diopside and hedenbergite, up to pure aegirine compositions (Reguir et al. 2012). At its peak, the hedenbergite component can consist of between 20 mol% and 40 mol% of a single clinopyroxene composition. The cause of the diopside–hedenbergite–aegirine trend is not discussed in detail by Reguir et al. (2012); instead, they ascribed it in passing to the "course of magma evolution". We would like to emphasise that this trend does not necessarily indicate an evolutionary process, but may instead simply record the possible range of clinopyroxene compositions in carbonatite systems. This compositional range is achieved because silica contamination can occur in different stages of carbonatite melt evolution, as it intrudes into whatever silicate lithologies happen to be at the site of carbonatite magmatism.

Clinopyroxene composition ranges achieved in our modelling are presented in Fig. 8. We only include the N, A, and K models in Fig. 8 because the S model would be a horizontal line connecting diopside and hedenbergite along the ternary edge. The S model is the only one which models the silica contamination process, whereas the other models (N, A, and K) explore compositional variations in an already contaminated rock. It is likely that a model combining both aspects would be able to replicate the observed

natural compositions close to the diopside endmember. Portions of our modelled compositional range agree with natural observations (Reguir et al. 2012). First, potassic models significantly overlap with natural aegirine-poor compositions (Fig. 8). This indicates the capacity of phlogopite to extract Mg from all other minerals, and strongly push clinopyroxene into hedenbergite-rich compositions. For non-potassic compositions there is very little overlap. Nonetheless, we find that low temperature and high pressure sodic models (N and A at < 600 °C and ≥ 3 kbar) reach the natural clinopyroxene field. We note that our modelled composition has a nominal equal molar mix of calcite and dolomite. In natural systems, sodic compositions are typically reached after protracted magmatic differentiation that fractionated Mg, either as dolomite or as Mg-rich antiskarn silicate minerals. The difficulty of achieving hedenbergite-rich clinopyroxenes could be simply the result of our predetermined Mg-rich composition. An examination of the host rocks for the hedenbergite-rich compositions in Reguir et al. (2012) confirms our suspicion that they contain few, if any, Mg-rich silicate minerals, other than phlogopite. Since ferromagnesian micas are ubiquitous in carbonatites, our K models are better suited to simulate natural carbonatite compositions.

Interestingly, Reguir et al. (2012) reports that the clinopyroxenes covered by their review are solely found in calcite carbonatite samples, often within their silicocarbonatitic parts. No predominantly-calcic clinopyroxenes are found in dolomite carbonatites (see also calcite carbonatites hosted within pyroxenites described by Ackerman et al. 2017). This is consistent with our Na-free model (S0–S1, Fig. 3) showing that there are no stable assemblages of dolomite and clinopyroxene at magmatic temperatures (> 600 °C), whereas these two phases may be cogenetic at lower temperatures. In contrast, clinopyroxene + dolomite assemblages are stabilised to higher temperatures in our Na-bearing

models, albeit over a limited compositional range (N and A, Figs. 4 and 5). The increased stability of clinopyroxene and dolomite in the Na-bearing model is probably the result of the lower silica activities relative to the Na-free model (Fig. 4). The two most aegirine-rich localities discussed by Reguir et al. (2012), Aley and Murun, do contain dolomite (Chakhmouradian et al. 2016b), but their association with aegirine is unclear. These observations can be extended to hydrous assemblages. For example, Hogarth (2016) describes dolomite carbonatites that contain very little silicates, and calcite carbonatites with abundant phlogopite, magnesio-riebeckite and magnesio-arfvedsonite. These calcite silicocarbonatites occur at the contact with surrounding quartz-bearing granitoids, whereas the dolomite carbonatites are found deeper inside the carbonatites (Hogarth 2016).

The Belaya Zima plutonic complex in Russia provides an example consistent with our Na-rich model compositions. It is characterised by the classic ring-like carbonatite structure with ankerite carbonatites in the core, surrounded by dolomite carbonatites, and finally rimmed by calcite carbonatites (Doroshkevich et al. 2016, 2017). Clinopyroxene rocks of the ijolite series occur around the various carbonatites at the contact with the silicate rocks (Doroshkevich et al. 2017). Here, clinopyroxene occurs in the same rocks as dolomite, apparently in contradiction with the dolomite–clinopyroxene exclusion principle discussed above. However, The Belaya Zima rocks are highly rich in alkaline phases such as burbankite and hilairite. Clinopyroxene reaches compositions very close to pure aegirine in these carbonatites. The high alkalinity suppresses the increase in silica activity as SiO_2 is introduced into the system, as is shown in Fig. 4. Our model permits the coexistence of dolomite–ankerite and clinopyroxene in alkaline compositions, as long as it is of roughly aegirine composition (Fig. 4). This is consistent with mass balance considerations as both dolomite and
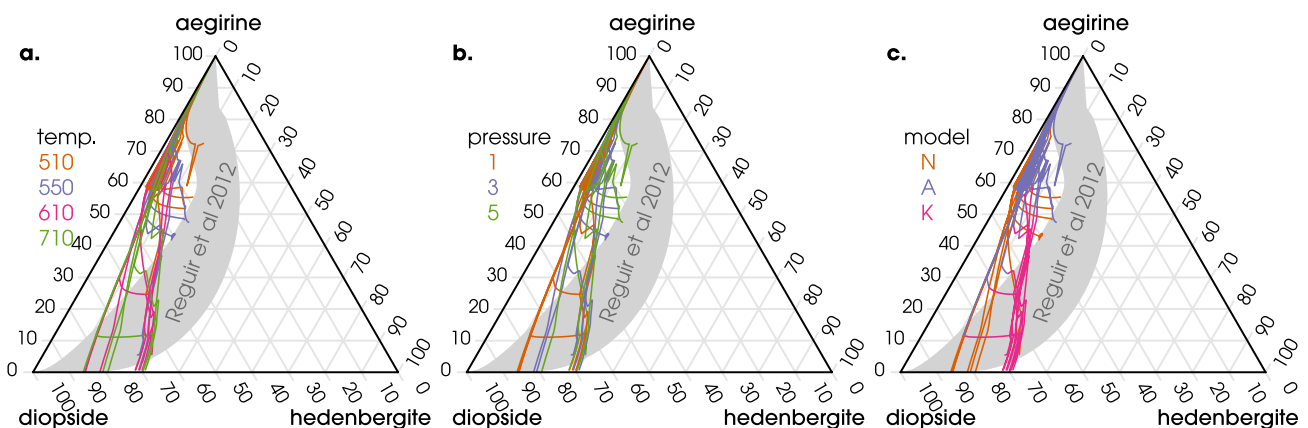

Fig. 8 Clinopyroxene compositions along isobaric and isothermal sections of models N, A, and K. Carbonatite-hosted clinopyroxene data from Reguir et al. (2012) shown for comparison as the grey area

diopside compete for Mg. Adding silica results in dolomite breakdown to diopside, but if Na and Fe^{3+} are available, silica addition will form aegirine instead, leaving Mg available for other phases. Similar relationships occur at the Montviel, Baikal, and Storkwitz complexes, in which nearly pure aegirine coexists with ankerite in ferrocarbonatites (Loidolt et al. 2023; Nadeau et al. 2016; Savelyeva et al. 2016).

Our modelling shows that the presence of Na-poor clinopyroxene indicates relatively high silica activities, particularly when close to diopside composition. Inasmuch as the widespread formation of clinopyroxene indicates silica contamination, the opposite also holds: Small amounts of xenocrystic clinopyroxene introduced to an uncontaminated carbonatite system will destabilise, as the system is still buffered to low silica activities and cannot support clinopyroxene (e.g., Barker 2001). For instance, Giebel et al. (2019) describes almost pristine clinopyroxene from a silica-contaminated carbonatite (the Badberg intrusion at Kaiserstuhl), but corroded clinopyroxene from silica-uncontaminated carbonatites (found at other Kaiserstuhl intrusions). Similarly, Chakhmouradian et al. (2008) shows that calcite carbonatites from Eden Lake contain abundant silicates indicative of high silica activity (titanite, feldspars, zircon, Barker 2001). They suggest that some of these silicates are xenocrysts derived from the surrounding silica-saturated rock. The Eden Lake carbonatites contain no dolomite, but abundant clinopyroxene and other Ca-Mg–silicates—an observation that we interpret as the formation of an antiskarn. Silica derived from the siliceous host rocks reacted with the dolomitic component in the carbonatite melt to form the Ca-Mg–silicates, and permitting solely calcite as the stable carbonate mineral (Fig. 3). Similar relationships are also observed in Twihinate (Bouabdellah et al. 2022) and Jacupiranga (Chmyz et al. 2022).

The carbonatite–pyroxenite and ijolite association

A common feature of carbonatite intrusions is their association with clinopyroxenites, which occasionally surround the carbonatite at the contact with the host silicate rocks, or appear in other ring-like structures (Ackerman et al. 2017; Beccaluva et al. 2017; Brassinnes et al. 2005; Chakhmouradian and Zaitsev 2002; Chen and Simonetti 2014; Cherbal et al. 2019; Cooper and Reid 1998; Doroshkevich et al. 2017; Hode Vuorinen et al. 2005; Nadeau et al. 2016; Nasir et al. 2003; Prokopyev et al. 2021; Savard and Mitchell 2021; Viladkar 2017). Most often, these clinopyroxenites contain some amount of nepheline. These clinopyroxene–nepheline rocks form the ijolite series. Ijolites usually contain minor amounts of calcite, and varieties with substantial calcite contents at > 10% are termed hollaites.

Ijolites and related rocks are often interpreted as the crystallisation products of alkaline silicate melts, whether these melts are the original liquids from which an immiscible carbonatite separated, or less related silicate melts which happen to occur at the same locality (Beccaluva et al. 2017; Chen and Simonetti 2014; Gittins and Harmer 2003; Groulier et al. 2020; Harmer 1999). Moreover, as experimental evidence shows that some carbonated silicate melts can fractionate to the point where they crystallise calcite as an igneous mineral (Brooker and Kjarsgaard 2011; Kjarsgaard 1998), it has been suggested that some carbonatites associated with ijolites are the direct result of ijolite formation, without distinct immiscibility (Brassinnes et al. 2005; Doroshkevich et al. 2016; Savard and Mitchell 2021; Veksler et al. 1998; Wu et al. 2017).

Even though ijolites are hypothesised to form from silicate melts, there is a paradoxical paucity of silicate melt inclusions in some ijolite-hosted minerals. Instead, a common melt inclusion type found within ijolites and related rocks is a carbonatite melt: an assortment of Na–K–Ca carbonates, halides, sulfates, and other minor phases (Fall et al. 2007; Guzmics et al. 2012; Isakova et al. 2015; Káldos et al. 2015; Le Bas and Aspden 1981; Nielsen et al. 1997; Prokof'ev et al. 2005; Rankin and Le Bas 1974; Sekisova et al. 2015; Veksler et al. 1998), which are often indistinguishable from melt inclusions found in proper carbonatites (Chayka et al. 2021; Chen et al. 2013; Fan et al. 2004a; Guzmics et al. 2019, 2011). The common coexistence of these carbonatite melts with immiscible silicate melts is often given as convincing evidence for carbonatite–silicate immiscibility (Guzmics et al. 2012; Rankin and Le Bas 1974; Veksler et al. 1998). Alternatively, these rocks have been described as individual magma pulses of varying compositions and their mutual mixing and mingling, such as at the Oka carbonatite complex (Chen and Simonetti 2014; Chen et al. 2016). However, the presence of carbonatite melt inclusions in ijolites could indicate that these and related rocks could have formed directly from the carbonatite melt, as was suggested by Vasyukova and Williams-Jones (2022).

Our results show that clinopyroxenites can form by addition of silica to a carbonatite, or alternatively by adding a carbonatite composition to a silicate rock (approximated here by 100% SiO_2). For example, extrapolation to higher SiO_2 of the model shown in Fig. 3 will result in a rock dominated by clinopyroxene with minor calcite. With increasing silica activity, dolomite would be exhausted to form calcite and olivine, followed by exhaustion of this newly-formed olivine and calcite to make clinopyroxene (Fig. 3). Participation of Al_2O_3 in the contamination process leads formation of nepheline as major rock forming mineral (Fig. 7). This assemblage of clinopyroxene, nepheline, and minor calcite is namely an ijolite, and at higher calcite contents would be a hollaite. As these silicate-forming reactions lead to substantial decarbonation (Fig. 3, Supp Figs. 1–6, Reaction (1)), H_2O would be significantly diluted leading to lower H_2O

activities (Supp Figs. 1–6) and preventing copious crystal-lisation of hydrous phases such as amphiboles or micas, in agreement with the mostly anhydrous mineral assemblage of ijolites (although later hydration of the anhydrous assemblage to amphiboles is often observed, for example at Montviel, Nadeau et al. 2016). This contrasts with lower temperature H_2O-rich fluids in which aegirine is unstable relative to alkali amphiboles such as riebeckite and arfvedsonite (Bailey 1969; Ernst 1962). Therefore, ijolites may be metasomatic rocks, forming without the presence of any silicate melts. The chiefly anhydrous clinopyroxene–nepheline assemblage is consistent with the interpretation of Vasyukova and Williams-Jones (2022) that the ijolite rock family represent high temperature metasomatic reaction between early carbonatite melts and siliceous wall rocks. They are potentially antiskarns—rocks formed by leaching of chemical components from the surrounding silicate rocks, and deposition as silicate minerals at the margins of the carbonatite melt conduit or chamber. Textural support is provided Anenburg and Mavrogenes (2018) who experimentally showed that clinopyroxene consistently forms at or close to the silicate–carbonatite interface, whereas olivine forms farther away inside the carbonatite (Anenburg and Mavrogenes 2018). This association is often observed in nature, where clinopyroxene forms on the conduit walls whereas olivine forms part of the carbonatite rock itself (Wei et al. 2020).

Rare earth element (REE) patterns observed in ijolites are also consistent with a metasomatic origin. Anenburg et al. (2020a) studied the REE contents of apatite and clinopyroxene from an antiskarn at Nolans Bore, Australia. The Nolans Bore clinopyroxene has a characteristic carbonatite-like sinusoidal pattern in which La–Ce are flat or gently sloping up until a maximum at Pr or Nd, then a negative slope down and an additional inflection point at Er–Tm, with a final increase to Lu. The Nolans Bore apatite is strongly light REE enriched, with La and Ce at roughly × 10,000 relative to chondrite, whereas the HREE are much less abundant with Yb and Lu at only about × 100 relative to chondrite. These patterns are nearly identical to patterns observed in apatite and clinopyroxene patterns from ijolites elsewhere, such as Jacupiranga (Beccaluva et al. 2017), Alnö (Hode Vuorinen et al. 2005), Prairie Lake and Fen (Savard and Mitchell 2021), as well as non-sodic pyroxenites (Su et al. 2023). Anenburg et al. (2020a) explained the sinusoidal shape to result from high CaO activities, such as those encountered in carbonatites. The same conclusion was reached by Hode Vuorinen et al. (2005) for their clinopyroxenites, which is hard to justify for a low-Ca alkaline silicate melt, ergo a carbonatite origin is more likely.

Glimmerites

In addition to the common association of carbonatites and sodic ijolites, some carbonatites are surrounded or contain biotite-dominated rocks called glimmerites. Like ijolites, they are common as rims of carbonatite ring structures, but also occur as replacements of wall rock xenoliths (hence interpreted as fenites). The Ngualla complex in Tanzania includes glimmerite facies, mostly associated with calcite carbonatite (Witt et al. 2019), in agreement with our model predicting that biotite is predominantly stable in the dolomite-free field (Fig. 6a). Nonetheless, the dolomite carbonatites of Ngualla contain minor biotite, which coexist with strongly ferroan dolomite and ankerite, again consistent with the Fe-rich composition of our modelled dolomite, in the limited T–X region where it is stable (Supp Fig. 22e, 25e). Interestingly, Witt et al. (2019) report clintonite, a brittle mica, which was experimentally found to form in antiskarns by Anenburg and Mavrogenes (2018). A low temperature demonstration of glimmerite formation can be found in the Yangibana carbonatites in Western Australia, which contain glimmerite reaction zones between Mg-poor ankerite–siderite dykes and the wall rocks (Slezak et al. 2021). Siilinjärvi in Finland is another example where silica contamination is likely to have occurred, with the rocks essentially lying along an continuum between phlogopite glimmerite and calcite carbonatite, with dolomite being both rare and Fe-bearing, if present (Al Ani 2013; Mattsson et al. 2019; O'Brien et al. 2015). Elsewhere, glimmerites are likewise mostly associated with calcite carbonatites, in agreement with dolomite instability during contamination of potassic rich systems (Beard et al. 1996; Nadeau et al. 2016; Pdah and Khonglah 2022).

Magnesium in calcite and olivine

Our modelling reveals that for alkali poor systems, the Mg content of calcite is a good indicator for silica contamination (Fig. 3f). Most carbonatite melts contain dissolved Mg, often measured in several wt% (Yaxley et al. 2022), and in the absence of silica, this Mg will partition to any crystallising calcite, as well as dolomite at more advanced stages of magmatic differentiation (Yaxley et al. 2022). This magnesian component is often observed as dolomite exsolution lamellae in calcite, as high-Mg igneous calcite is not stable at ambient temperatures (Chakhmouradian et al. 2016b; Chmyz et al. 2022; Zaitsev and Polezhaeva 1994). However, calcite Mg contents in our models drop rapidly with the introduction of silica (Fig. 3f). For example, Giebel et al. (2019) studied several carbonatites from Kaiserstuhl,

Germany. They show that Badberg, a silica-contaminated carbonatite with abundant diopside-rich clinopyroxene, contains calcite in which MgO is essentially zero. All other carbonatites from Kaiserstuhl are uncontaminated, and contain between 0.5 and 1.5% MgO. Giebel et al. (2019) suggested that silica contamination leads to formation of Mg-rich mica which depletes the calcite of Mg. Our study confirms this and demonstrates that Mg is preferentially partitioned to silicate phases relative to carbonate phases. This effect is most obvious in the case of biotite (Supp Figs. 19–27), consistent with the observations of Giebel et al. (2019). In contrast, Wei et al. (2020) show forsterite-calcite carbonatites with only minor silica contamination. There, the low amount of silica only allowed olivine formation instead clinopyroxene, leaving minor amounts of residual dolomite (See low X_{S1} in Fig. 3a). In this case, some of the MgO remained in calcite (Fig. 3f). The residual dolomite has lower ankerite components compared to the associated uncontaminated dolomite carbonatite, consistent with our models (Supp Figs. 1–6).

Choudhary et al. (2021) claimed that carbonatite-hosted Mg-rich olivine comes from the mantle. Alternatively, Li et al. (2018) implicated Mg-rich olivine in assimilation of ultramafic xenoliths. However, these forsterite-dominated olivines are stabilised in our model and are commonly interpreted to readily form in carbonatites (Giebel et al. 2019; Guarino et al. 2017; Guzmics et al. 2011; Mikhailova et al. 2018; Plechov et al. 2018; Xie et al. 2019). These occurrences demonstrate the thermodynamic stability of forsterite and calcite at upper crustal conditions without the need to invoke xenocrysts or any ultramafic influence.

Magnetite, aegirine, and formation of reduced phases

Formation of aegirine requires Fe^{3+}, presumably sourced from Fe^{3+} dissolved in the carbonatite melt. Our model does not consider carbonatite melts, but the magnetite component of spinel reflects this relationship well. In our Na-bearing model (N0–N1), magnetite is predicted to be stable with diopside-rich clinopyroxene (low X_{N1} in Fig. 4a, d), which is observed in some carbonatites where magnetite and clinopyroxene are cogenetic (Reguir et al. 2012). From N0 to N1, Na_2O is increased at constant SiO_2. In our models we also fix the excess O_2 content (primarily associated with Fe_2O_3 and CO_2) to a constant value. Carbon and Fe are the only redox sensitive elements in our calculation. As a response to the increase in Na_2O contents, Fe^{3+} is partitioned into clinopyroxene while destabilising magnetite (Fig. 4a, d). Magnetite and aegirine rarely coexist in carbonatites, consistent with this prediction (e.g., Groulier et al. 2020).

Fluid inclusions in some carbonatites contain abundant H_2O and CO_2, but rare CH_4 is occasionally observed typically associated with alkaline mineral assemblages (Bühn
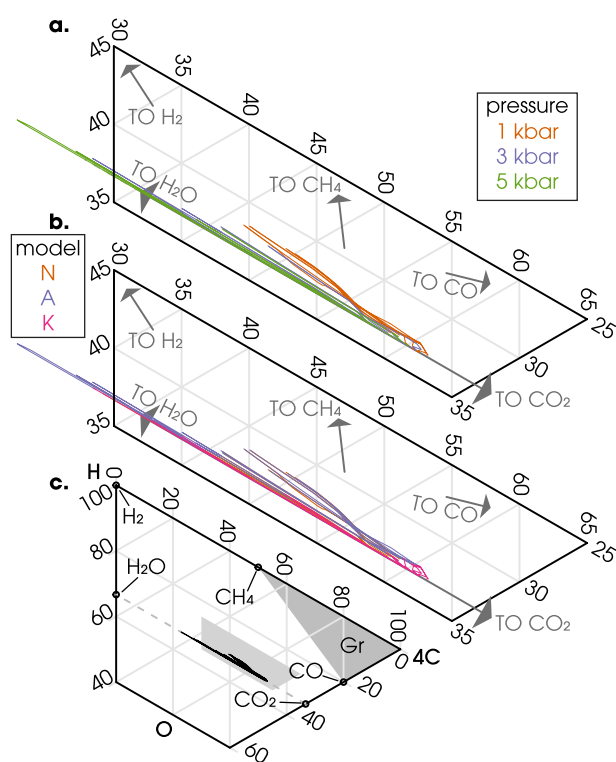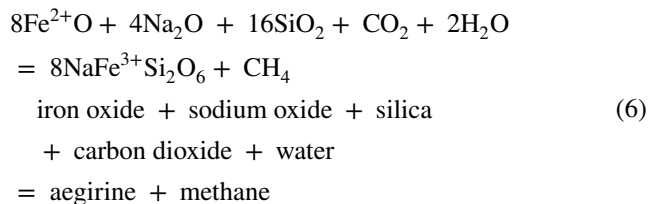

Fig. 9 The range of fluid compositions derived from temperature sections through all models at 100, 300, and 500 MPa and 510, 550, 610, and 710 °C. Temperature was found to have no effect, so it is not shown here for simplicity. The location of **a** and **b** is marked on shaded area in the **c** ternary

and Rankin 1999; Cangelosi et al. 2020; Dowman et al. 2017; Fan et al. 2004b; Hurai et al. 2021; Nivin et al. 2005; Ryabchikov and Kogarko 2009; Ryabchikov et al. 2008; Ting et al. 1994; Walter et al. 2021; Williams-Jones and Palmer 2002). Natural systems invariably contain abundant H_2O, and therefore the H-absent aegirine-forming Reactions 2 and 3 predicted in our Na-bearing model may not fully apply in nature. Instead, Fe^{3+} in aegirine may form by reducing CO_2 to CH_4 through reactions in the general form of:

$$8Fe^{2+}O + 4Na_2O + 16SiO_2 + CO_2 + 2H_2O$$

$$= 8NaFe^{3+}Si_2O_6 + CH_4$$

$$\text{iron oxide} + \text{sodium oxide} + \text{silica} \qquad (6)$$

$$+ \text{ carbon dioxide} + \text{water}$$

$$= \text{ aegirine} + \text{methane}$$

Evidence that this reaction is thermodynamically favourable is observed by the increase in CH_4 contents upon introduction of Na_2O in our N0–N1 models (Fig. 4c, Supp Figs. 7–12). Such reactions may remove FeO from the melt, but also destabilise Fe^{2+}-bearing phases such as hedenbergite and magnetite. An important property of Reaction 6 is

that 8 mol of FeO are oxidised and 4 mol of Na_2O are consumed for each mole of C reduced. Given that carbonatites have over an order of magnitude greater CO_2 compared to FeO on a molar basis, Reaction 6 could potentially cease due to FeO exhaustion. Thus, the range of C oxidation states and their abundance exhibit a significant leverage over Fe. The relationship of CO_2, H_2O, and CH_4 with fO_2 can be described by the following equilibrium:

$$CO_2 + H_2O = CH_4 + O_2$$
$$\text{carbon dioxide} + \text{water} = \text{methane} + \text{oxygen} \quad (7)$$
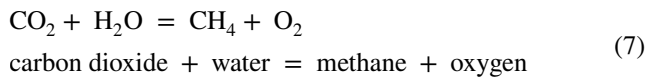
where fO_2 will evolve as the proportions of CO_2, H_2O, CO, and CH_4 in the fluid change, as dictated by mineral-fluid equilibria, such as Reaction 6. The fluid composition is predicted to vary as a function of the Na_2O content as shown in the C-O–H ternary in Fig. 9, where fO_2 is lowest and H_2O contents are highest at high X_{N1} (see also Supp. Figure 12d, f). In natural systems, aegirine crystallisation through Fe oxidation and C reduction (Reaction 6) will decrease the O/H proportion in the fluid by consuming H_2O and CO_2. As a result, fO_2 will decrease as Reaction 9 progresses and determines the C-O–H fluid composition. This, in turn, buffers fO_2 through the equilibrium in Reaction 7. This scenario is in sharp contrast to previous work by Morogan (1994), where the formation of aegirine was explained to result from increasing fO_2. Instead, aegirine formation is predicted here to be accompanied by a decrease in fO_2 (Fig. 4b). Similar processes have been shown to lead to formation of aegirine–methane pairs in sodic peralkaline silica-undersaturated silicate systems (Markl et al. 2010). At low temperatures and high H_2O contents, formation of riebeckite and arfvedsonite (Na and Fe^{3+}-rich amphiboles) instead of aegirine might lead to even lower fO_2 values (Bailey 1969; Ernst 1962). One might argue that formation of reduced species is inevitable in our modelling solely because of mass balance considerations—that alkali amphiboles and aegirine are the only suitable sodium silicates existing in the thermodynamic database to accommodate Na, Fe, and Si (Holland and Powell 2011). However, even with the introduction of Al_2O_3 in the A0–A1 model, these sodic ferromagnesian minerals are still stable. Indeed, they are no longer sodic endmembers (Fig. 5) but still contain considerable Na–Fe^{3+} components, in excess of the Fe^{3+} initially available from magnetite. Thus, they remain stable and retain their reductive influence on carbon despite the stability of alkali aluminosilicates such as feldspars and nepheline.

The above discussion mostly focused on reduced fluid species, but our models also predict widespread existence of graphite over a wide range of temperatures at sodic compositions (Fig. 4a). Graphite is not often considered a typical mineral for carbonatites, but this could result from the simple fact that unless it is well crystallised, graphite is frequently overlooked in petrographic studies. Nevertheless, graphite has been reported in some carbonatites. Doroshkevich et al. (2007) document graphite with mantle-like $\delta^{13}C$ values, which they interpret as magmatic crystallisation from a Fe^{2+}-rich carbonatite. Their rocks also contain almost pure aegirine, consistent with our modelling of a Na-rich system as a requirement for graphite formation. Also of interest are textures observed in the Newania carbonatites, where graphite likewise coexists with Fe-rich carbonates and aegirine (Doroshkevich et al. 2010). These rocks also contain magnetite, which according to our modelling should be mutually exclusive with graphite (Fig. 4a). However, the textures reported by Doroshkevich et al. (2010) indicate possible disequilibrium whereby graphite occurs as coating around magnetite grains, or in seemingly replacement textures. Additional graphite has been reported from clinopyroxene-bearing silicocarbonatites elsewhere (Shumilova et al. 2013).

This process demonstrates an important point regarding redox exchanges. The appearance of reduced carbonic species and the drop in oxygen fugacity do not mean that the system is any more reduced than before (e.g., Walter et al. 2021; Williams-Jones and Palmer 2002). This is particularly surprising as carbonatites are considered to be some of the most oxidised out of all alkaline magmas (Braunger et al. 2020). The bulk amount of oxygen initially associated with redox sensitive species has not changed in our models (i.e., O_2 in SiO_2 is added to the system but does not participate in any redox transformations). We show that the addition of redox inert components, like SiO_2 and Na_2O, drives the crystallisation of phases via modulating the partitioning of Fe^{2+} and Fe^{3+}, as well as redox reactions that can convert Fe^{2+} to Fe^{3+}. However, if the system remains closed (i.e., CH_4 is not lost after it is produced) then the system itself is not 'reduced' or 'oxidised' in response to the redox reactions. Quantitative removal of CH_4 would oxidise the system following Reaction 6, a process that may occur in nature. We find that in carbonatites, the presence of Na, Fe, and Si requires that aegirine or its amphibole equivalents form, which in turn imposes the presence of Fe^{3+}. The stability of these minerals overwhelms the otherwise overall oxidised environment, paradoxically leading to the formation of reduced fluid and carbonic phases even though all Fe is trivalent. This is counterintuitive in that aegirine and alkali amphiboles, being Fe^{3+} minerals, are often associated with more oxidised systems (Ventura et al. 2023; Yagi 1966), but can exist in our circumstances alongside reduced carbon species (thus completing the Fe–C redox couple). This point is made clearer in our K models where K replaces Na on an atom-by-atom basis, while all other chemical components remain identical. Remarkably, this replacement leads to a drastic increase in oxygen fugacity and disappearance of graphite and reduced C–O–H fluid components (Fig. 6a,

b), despite no changes whatsoever to the amounts of redox sensitive elements such as Fe, C, or O.

A second important point is that oxygen fugacity is not a driver of chemical change, but rather a monitor of the chemical potential of O_2. Thus, fO_2 depends on many other factors besides simple redox reactions, such as stable phase assemblage, bulk composition, P, and T. It is worthwhile to remember that in most petrological systems O_2 is a thermodynamic chemical component (i.e., a mathematical construct), and does not actually exist as a phase in the system. Lower fO_2 does not necessarily mean that bulk reduction has occurred (Anenburg and O'Neill 2019).

Limitations and outlook

Our study provides supporting evidence, rooted in thermodynamics, that silicate minerals in crustal carbonatites are likely to have formed because of siliceous wall rock contamination. The mineral assemblages and compositional variations predicted here are largely consistent with observations from natural rocks. Notwithstanding these strengths, there are some limitations to our thermodynamic modelling. Perhaps the most obvious is that we model a liquid-bearing igneous system without including a melt phase. Although in this case we are assuming the multiple solid phase saturation buffers the liquid composition, it would be beneficial to have a carbonatite melt model such that contamination processes can be reliable at higher temperatures with less solid minerals, or to combine such modelling with igneous fractionation models. Phase stability ranges will also improve because any currently stable phases might be entirely soluble in a hypothetical liquid phase, ceasing their ability to buffer reactions and compositions. Any carbonatite melt model will have to include some of the more common rock-forming minerals in carbonatites such as apatite, nyerereite, fluorite, baryte, and gregoryite. Furthermore, some models we used do not cover the full compositional range observed in carbonatites, such as lack of F in biotite (e.g., Giebel et al. 2019), and Sr in calcite and dolomite (Chakhmouradian et al. 2016a). Although the Na–Fe^{3+}-rich compositions of the clinopyroxene and amphibole models used here—Omph(GHP) and cAmph(G)—are sufficiently reasonable (E.C.R. Green, pers. comm.), additional calibration and validation for aegirine, arfvedsonite and riebeckite will contribute to the model accuracies. Finally, in the three years since we began working on this thermodynamic modelling and final submission of the manuscript, the Perple_X software package underwent major updates, upgrades, and bug fixes. These advances were undoubtedly instrumental to the success of the thermodynamic models presented here. This discussion ostensively demonstrates that further development of thermodynamic software, data, and models relevant to carbonatite systems will be highly beneficial.

General compositional and mineralogical trends

Many of the concepts discussed above are readily applied in the study of natural rocks. For instance, the recent example of Fengzhen in the North China Craton is particularly relevant (described in the appropriately titled paper: "when carbonatite met granite", Su et al. 2023). At Fengzhen, calcite carbonatite intrusions into aluminous granite are accompanied by zones of pyroxenite with minor syenite blocks. Geochemically, the pyroxenites are intermediate between carbonatites and granites. The pyroxenite mineral assemblage is dominated by diopside–hedenbergite, K-feldspar, phlogopite, and olivine. This mineral assemblage is remarkably like our K model, with the exception that at Fengzhen, amphibole is absent whereas olivine coexists with phlogopite. We explain this by lower Al_2O_3 contents at Fengzhen, in which the carbonatite melt assimilated a quartz–feldspar assemblage containing a much higher Si:Al ratio than introduced in our A model (Si:Al of 1:1). Su et al. (2023) also report that oxygen fugacity values at Fengzhen were greater than FMQ, consistent with their almost Na_2O-free rocks and our K model close to its potassic end ($X_{K1} = 1$). Similar characteristics are observed at the Sung Valley carbonatite (Gogoi and Hazarika 2023), where a silica contamination origin have not been suggested but is likely to have occurred.

Generalisation of our results to natural rocks leads to several guidelines or rules of thumb. The compositional variations and equilibrium states observed in Figs. 3, 4, 5 and 6 (for 3 kbar) and the Supplementary Figures (for other pressures) indicate several trends of note:

1. A contaminated carbonatite will typically contain carbonate minerals with higher Fe/Mg compared to a compositionally equivalent uncontaminated carbonatite.
2. In an alkali-rich system, the lack of magnetite and presence of Fe^{3+}-bearing silicates such as alkali amphibole, aegirine, or tetraferriphlogopite is a strong indicator for silica contamination.
3. In an alkali-poor system, an uncontaminated carbonatite will contain a higher magnesioferrite component in the magnetite, compared to purer magnetite in a contaminated carbonatite.
4. Coexistence of dolomite and Mg-rich olivine in a contaminated carbonatite occurs over a very narrow temperature range of roughly 600 to 650 °C (at 3 kbar) and can serve as a thermometer. In an uncontaminated carbonatite (i.e., containing only small amount of olivine

and no other silicates) their coexistence may indicate higher temperatures.

5. If no micas or other potassic phases are found, albite or nepheline reliably indicate temperatures lower or higher than ~ 600 °C, respectively. The boundary rises to ~ 750 °C with introduction of K_2O. Nonetheless, a temperature range of 150 °C is sufficient to differentiate some petrogenetic processes.

6. In systems with both Na and K, perthite exsolutions in alkali feldspars are reliable indicators for high pressures, because nepheline truncates the solvus at low pressures. This leads to formation of two feldspars instead.

7. Amphibole is stabilised in alumina-rich systems to high temperatures, and will often sequester more Na–Fe^{3+} than coexisting clinopyroxenes. This indicates that riebeckite or arfvedsonite can be stable and coexist with only moderately sodic clinopyroxenes (i.e., aegirine-augite).

8. Graphite coexisting with a Fe^{3+}-bearing silicate is a reliable indicator of silica contamination of an alkaline carbonatite without sufficient initial Fe^{3+} to accommodate all currently present silicates. Methane is likely to be generated and potentially trapped in fluid inclusions.

9. Quartz is highly unlikely to form from Fe-rich carbonatite melts. Quartz can form at subsolidus conditions via reequilibration induced by hydrothermal or metamorphic activity.

References

Ackerman L, Magna T, Rapprich V, Upadhyay D, Krátký O, Čejková B, Erban V, Kochergina YV, Hrstka T (2017) Contrasting petrogenesis of spatially related carbonatites from Samalpatti and Sevattur, Tamil Nadu, India. Lithos 284–285:257–275. https://doi.org/10.1016/j.lithos.2017.03.029

Al Ani T (2013) Mineralogy and petrography of Siilinjärvi carbonatite and glimmerite rocks, eastern Finland. Geol Surv Finland Rep 164:2013. https://tupa.gtk.fi/raportti/arkisto/164_2013.pdf

Anenburg M, Guzmics T (2023) Silica is unlikely to be soluble in upper crustal carbonatite melts. Nat Commun 14(1):942. https://doi.org/10.1038/s41467-023-35840-6

Anenburg M, Mavrogenes JA (2018) Carbonatitic versus hydrothermal origin for fluorapatite REE-Th deposits: experimental study of REE transport and crustal "antiskarn" metasomatism. Am J Sci 318(3):335–366. https://doi.org/10.2475/03.2018.03

Anenburg M, O'Neill HSC (2019) Redox in magmas: comment on a recent treatment of the Kaiserstuhl Volcanics (Braunger et al., Journal of Petrology, 59, 1731–1762, 2018) and some other misconceptions. J Petrol 60(9):1825–1832. https://doi.org/10.1093/petrology/egz046

Anenburg M, Mavrogenes JA, Bennett VC (2020a) The fluorapatite P–REE–Th vein deposit at Nolans Bore: genesis by carbonatite metasomatism. J Petrol 61(1):egaa003. https://doi.org/10.1093/petrology/egaa003

Anenburg M, Mavrogenes JA, Frigo C, Wall F (2020b) Rare earth element mobility in and around carbonatites controlled by sodium, potassium, and silica. Sci Adv 6(41):eabb6570. https://doi.org/10.1126/sciadv.abb6570

Anenburg M, Broom-Fendley S, Chen W (2021) Formation of rare earth deposits in carbonatites. Elements 17(5):327–332. https://doi.org/10.2138/gselements.17.5.327

Bailey DK (1969) The stability of acmite in the presence of H_2O. Am J Sci 267-A:1–16. http://earth.geology.yale.edu/~ajs/SchairerVol.html

Barker DS (2001) Calculated silica activities in carbonatite liquids. Contrib Miner Petrol 141(6):704–709. https://doi.org/10.1007/s004100100281

Beard AD, Downes H, Vetrin V, Kempton PD, Maluski H (1996) Petrogenesis of Devonian lamprophyre and carbonatite minor intrusions, Kandalaksha Gulf (Kola Peninsula, Russia). Lithos 39(1–2):93–119. https://doi.org/10.1016/s0024-4937(96)00020-5

Beccaluva L, Bianchini G, Natali C, Siena F (2017) The alkaline-carbonatite complex of Jacupiranga (Brazil): magma genesis and mode of emplacement. Gondwana Res 44:157–177. https://doi.org/10.1016/j.gr.2016.11.010

Berndt J, Klemme S (2022) Origin of carbonatites—liquid immiscibility caught in the act. Nat Commun 13(1):2892. https://doi.org/10.1038/s41467-022-30500-7

Berndt J, Klemme S (2023) Reply to: silica is unlikely to be soluble in upper crustal carbonatite melts. Nat Commun 14(1):943. https://doi.org/10.1038/s41467-023-35841-5

Bouabdellah M, Boukirou W, Jébrak M, Bigot F, Yans J, Mouttaqi A, El Gadarri M, Errami A, Levresse G (2022) Discovery of antiskarn-hosted strategic metal mineralization in the Upper Cretaceous Twihinate carbonatite intrusion (West African Craton Margin, Moroccan Sahara). Ore Geol Rev 149:105105. https://doi.org/10.1016/j.oregeorev.2022.105105

Bowen NL, Tuttle OF (1950) The system $NaAlSi_3O_8$-$KAlSi_3O_8$-H_2O. J Geol 58(5):489–511. https://www.jstor.org/stable/30068566

Brady AE, Moore KR (2012) A mantle-derived dolomite silicocarbonatite from the southwest coast of Ireland. Mineral Mag 76(2):357–376. https://doi.org/10.1180/minmag.2012.076.2.06

Brassinnes S, Balaganskaya E, Demaiffe D (2005) Magmatic evolution of the differentiated ultramafic, alkaline and carbonatite intrusion of Vuoriyarvi (Kola Peninsula, Russia). A LA-ICP-MS study of apatite. Lithos 85(1–4):76–92. https://doi.org/10.1016/j.lithos.2005.03.017

Braunger S, Marks MAW, Wenzel T, Chmyz L, Guitarrari Azzone R, Markl G (2020) Do carbonatites and alkaline rocks reflect variable redox conditions in their upper mantle source? Earth Planet Sci Lett 533:116041. https://doi.org/10.1016/j.epsl.2019.116041

Brooker RA, Kjarsgaard BA (2011) Silicate–carbonate liquid immiscibility and phase relations in the system SiO_2–Na_2O–Al_2O_3–CaO–CO_2 at 0.1–2.5 GPa with applications to carbonatite genesis. J Petrol 52:1281–1305. https://doi.org/10.1093/petrology/egq081

Bühn B, Rankin AH (1999) Composition of natural, volatile-rich Na–Ca–REE–Sr carbonatitic fluids trapped in fluid inclusions. Geochim Cosmochim Acta 63(22):3781–3797. https://doi.org/10.1016/S0016-7037(99)00180-5

Cangelosi D, Smith M, Banks D, Yardley B (2020) The role of sulfate-rich fluids in heavy rare earth enrichment at the Dashigou carbonatite deposit, Huanglongpu, China. Mineral Mag 84(1):65–80. https://doi.org/10.1180/mgm.2019.78

Chakhmouradian AR, Zaitsev AN (2002) Calcite – amphibole – clinopyroxene rock from the Afrikanda Complex, Kola Peninsula, Russia: mineralogy and a possible link to carbonatites. III. Silicate minerals. Can Mineral 40(5):1347–1374. https://doi.org/10.2113/gscanmin.40.5.1347

Chakhmouradian AR, Mumin AH, Demény A, Elliott B (2008) Postorogenic carbonatites at Eden Lake, Trans-Hudson Orogen (northern Manitoba, Canada): geological setting, mineralogy and geochemistry. Lithos 103(3–4):503–526. https://doi.org/10.1016/j.lithos.2007.11.004

Chakhmouradian AR, Reguir EP, Couëslan C, Yang P (2016a) Calcite and dolomite in intrusive carbonatites. II. Trace-element variations. Mineral Petrol 110(2–3):361–377. https://doi.org/10.1007/s00710-015-0392-4

Chakhmouradian AR, Reguir EP, Zaitsev AN (2016b) Calcite and dolomite in intrusive carbonatites. I. Textural variations. Mineral Petrol 110(2–3):333–360. https://doi.org/10.1007/s00710-015-0390-6

Chayka IF, Kamenetsky VS, Vladykin NV, Kontonikas-Charos A, Prokopyev IR, Stepanov SY, Krasheninnikov SP (2021) Origin of alkali-rich volcanic and alkali-poor intrusive carbonatites from a common parental magma. Sci Rep 11(1):17627. https://doi.org/10.1038/s41598-021-97014-y

Chen W, Simonetti A (2014) Evidence for the multi-stage petrogenetic history of the Oka carbonatite complex (Québec, Canada) as recorded by perovskite and apatite. Minerals 4(2):437–476. https://doi.org/10.3390/min4020437

Chen W, Kamenetsky VS, Simonetti A (2013) Evidence for the alkaline nature of parental carbonatite melts at Oka complex in Canada. Nat Commun 4:2687. https://doi.org/10.1038/ncomms3687

Chen W, Zhang W, Simonetti A, Jian S (2016) Mineral chemistry of melanite from calcitic ijolite, the Oka carbonatite complex, Canada: implications for multi-pulse magma mixing. J Earth Sci 27(4):599–610. https://doi.org/10.1007/s12583-016-0715-3

Cherbal M, Yonezu K, Aissa DE, Tindell T, Watanabe K (2019) Metacarbonatite rocks from Amesmessa area (In Ouzzal Terrane), Hoggar shield, Algeria. J Afr Earth Sci 153:268–277. https://doi.org/10.1016/j.jafrearsci.2018.12.013

Chmyz L, Azzone RG, Ruberti E, Marks MAW, Santos TJSd (2022) Olivines as probes into assimilation of silicate rocks by carbonatite magmas: unraveling the genesis of reaction rocks from the Jacupiranga alkaline-carbonatite complex, southern Brazil. Lithos 416–417:106647. https://doi.org/10.1016/j.lithos.2022.106647

Choudhary S, Sen K, Kumar S, Rana S, Ghosh S (2021) Forsterite reprecipitation and carbon dioxide entrapment in the lithospheric mantle during its interaction with carbonatitic melt: a case study from the Sung Valley ultramafic–alkaline–carbonatite complex, Meghalaya, NE India. Geol Mag 158(3):475–486. https://doi.org/10.1017/s0016756820000631

Connolly JAD (1995) Phase diagram methods for graphitic rocks and application to the system C−O−H−FeO−TiO_2−SiO_2. Contrib Miner Petrol 119(1):94–116. https://doi.org/10.1007/bf00310720

Connolly JAD (2009) The geodynamic equation of state: what and how. Geochem Geophys Geosyst 10(10):Q10014. https://doi.org/10.1029/2009gc002540

Cook SJ, Bowman JR (2000) Mineralogical evidence for fluid–rock interaction accompanying prograde contact metamorphism of siliceous dolomites: Alta Stock aureole, Utah, USA. J Petrol 41(6):739–757. https://doi.org/10.1093/petrology/41.6.739

Cooper AF, Reid DL (1998) Nepheline sövites as parental magmas in carbonatite complexes: evidence from Dicker Willem, Southwest Namibia. J Petrol 39(11–12):2123–2136. https://doi.org/10.1093/petroj/39.11-12.2123

Crameri F (2018) Scientific colour maps. Zenodo. https://doi.org/10.5281/zenodo.1243862

Doroshkevich AG, Wall F, Ripp GS (2007) Magmatic graphite in dolomite carbonatite at Pogranichnoe, North Transbaikalia, Russia. Contrib Mineral Petrol 153(3):339–353. https://doi.org/10.1007/s00410-006-0150-z

Doroshkevich AG, Ripp G, Viladkar S (2010) Newania carbonatites, Western India: example of mantle derived magnesium carbonatites. Mineral Petrol 98(1–4):283–295. https://doi.org/10.1007/s00710-009-0076-z

Doroshkevich AG, Veksler IV, Izbrodin IA, Ripp GS, Khromova EA, Posokhov VF, Travin AV, Vladykin NV (2016) Stable isotope composition of minerals in the Belaya Zima plutonic complex, Russia: implications for the sources of the parental magma and metasomatizing fluids. J Asian Earth Sci 116:81–96. https://doi.org/10.1016/j.jseaes.2015.11.011

Doroshkevich AG, Veksler IV, Klemd R, Khromova EA, Izbrodin IA (2017) Trace-element composition of minerals and rocks in the Belaya Zima carbonatite complex (Russia): implications for the mechanisms of magma evolution and carbonatite formation. Lithos 284–285:91–108. https://doi.org/10.1016/j.lithos.2017.04.003

Dowman E, Wall F, Treloar PJ, Rankin AH (2017) Rare-earth mobility as a result of multiple phases of fluid activity in fenite around the Chilwa Island Carbonatite, Malawi. Mineral Mag 81(06):1367–1395. https://doi.org/10.1180/minmag.2017.081.007

Elliott HAL, Wall F, Chakhmouradian AR, Siegfried PR, Dahlgren S, Weatherley S, Finch AA, Marks MAW, Dowman E, Deady E (2018) Fenites associated with carbonatite complexes: a review. Ore Geol Rev 93:38–59. https://doi.org/10.1016/j.oregeorev.2017.12.003

Ernst WG (1962) Synthesis, stability relations, and occurrence of riebeckite and riebeckite-arfvedsonite solid solutions. J Geol 70(6):689–736. https://doi.org/10.1086/626866

Fall A, Bodnar RJ, Szabó C, Pál-Molnár E (2007) Fluid evolution in the nepheline syenites of the Ditrău Alkaline Massif, Transylvania, Romania. Lithos 95(3–4):331–345. https://doi.org/10.1016/j.lithos.2006.08.005

Fan H-R, Xie Y-H, Wang K-Y, Tao K-J, Wilde SA (2004a) REE daughter minerals trapped in fluid inclusions in the giant Bayan Obo REE-Nb-Fe deposit, Inner Mongolia, China. Int Geol Rev 46(7):638–645. https://doi.org/10.2747/0020-6814.46.7.638

Fan H-R, Xie Y-H, Wang K-Y, Wilde SA (2004b) Methane-rich fluid inclusions in skarn near the giant REE–Nb–Fe deposit at Bayan

Obo, Northern China. Ore Geol Rev 25(3–4):301–309. https://doi.org/10.1016/j.oregeorev.2004.05.001

Ferry JM, Blencoe JG (1978) Subsolidus phase relations in the nepheline–kalsilite system at 0.5, 2.0, and 5.0 kbar. Am Mineral 63(11–12):1225–1240. http://www.minsocam.org/msa/collectors_corner/amtoc/toc1978.htm

Franzolin E, Schmidt MW, Poli S (2011) Ternary Ca–Fe–Mg carbonates: subsolidus phase relations at 3.5 GPa and a thermodynamic solid solution model including order/disorder. Contrib Mineral Petrol 161(2):213–227. https://doi.org/10.1007/s00410-010-0527-x

Giebel RJ, Parsapoor A, Walter BF, Braunger S, Marks MAW, Wenzel T, Markl G (2019) Evidence for magma–wall rock interaction in carbonatites from the Kaiserstuhl Volcanic Complex (Southwest Germany). J Petrol 60(6):1163–1194. https://doi.org/10.1093/petrology/egz028

Gittins J, Harmer RE (2003) Myth and reality in the carbonatite - silicate rock "association." Periodico Di Mineralogia 72(1):19–26. https://www.dst.uniroma1.it/riviste/permin/spVol1_03.html

Gogoi R, Hazarika P (2023) Magmatic-hydrothermal evolution of the Sung Valley Carbonatite, northeastern India. J Earth Syst Sci 132(2):70. https://doi.org/10.1007/s12040-023-02089-y

Green E, Holland T, Powell R (2007) An order-disorder model for omphacitic pyroxenes in the system jadeite-diopside-hedenbergite-acmite, with applications to eclogitic rocks. Am Miner 92(7):1181–1189. https://doi.org/10.2138/am.2007.2401

Green ECR, White RW, Diener JFA, Powell R, Holland TJB, Palin RM (2016) Activity-composition relations for the calculation of partial melting equilibria in metabasic rocks. J Metamorph Geol 34(9):845–869. https://doi.org/10.1111/jmg.12211

Groulier P-A, Turlin F, André-Mayer A-S, Ohnenstetter D, Crépon A, Boulvais P, Poujol M, Rollion-Bard C, Zeh A, Moukhsil A, Solgadi F, El Basbas A (2020) Silicate-carbonate liquid immiscibility: insights from the Crevier alkaline intrusion (Quebec). J Petrol 61(3):egaa033. https://doi.org/10.1093/petrology/egaa033

Guarino V, Wu F-Y, Melluso L, de Barros GC, Tassinari CCG, Ruberti E, Brilli M (2017) U-Pb ages, geochemistry, C–O–Nd–Sr–Hf isotopes and petrogenesis of the Catalão II carbonatitic complex (Alto Paranaíba Igneous Province, Brazil): implications for regional-scale heterogeneities in the Brazilian carbonatite associations. Int J Earth Sci 106(6):1963–1989. https://doi.org/10.1007/s00531-016-1402-4

Guzmics T, Mitchell RH, Szabó C, Berkesi M, Milke R, Abart R (2011) Carbonatite melt inclusions in coexisting magnetite, apatite and monticellite in Kerimasi calciocarbonatite, Tanzania: melt evolution and petrogenesis. Contrib Miner Petrol 161(2):177–196. https://doi.org/10.1007/s00410-010-0525-z

Guzmics T, Mitchell RH, Szabó C, Berkesi M, Milke R, Ratter K (2012) Liquid immiscibility between silicate, carbonate and sulfide melts in melt inclusions hosted in co-precipitated minerals from Kerimasi volcano (Tanzania): evolution of carbonated nephelinitic magma. Contrib Miner Petrol 164(1):101–122. https://doi.org/10.1007/s00410-012-0728-6

Guzmics T, Zajacz Z, Mitchell RH, Szabó C, Wälle M (2015) The role of liquid–liquid immiscibility and crystal fractionation in the genesis of carbonatite magmas: Insights from Kerimasi melt inclusions. Contrib Miner Petrol 169(2):17. https://doi.org/10.1007/s00410-014-1093-4

Guzmics T, Berkesi M, Bodnar RJ, Fall A, Bali E, Milke R, Vetlényi E, Szabó C (2019) Natrocarbonatites: a hidden product of three-phase immiscibility. Geology 47(6):527–530. https://doi.org/10.1130/g46125.1

Harmer RE (1999) The petrogenetic association of carbonatite and alkaline magmatism: constraints from the Spitskop complex, South Africa. J Petrol 40(4):525–548. https://doi.org/10.1093/petroj/40.4.525

Hode Vuorinen J, Skelton ADL (2004) Origin of silicate minerals in carbonatites from Alno Island, Sweden: magmatic crystallization or wall rock assimilation? Terra Nova 16(4):210–215. https://doi.org/10.1111/j.1365-3121.2004.00557.x

Hode Vuorinen J, Hålenius U, Whitehouse MJ, Mansfeld J, Skelton ADL (2005) Compositional variations (major and trace elements) of clinopyroxene and Ti-andradite from pyroxenite, ijolite and nepheline syenite, Alnö Island, Sweden. Lithos 81(1–4):55–77. https://doi.org/10.1016/j.lithos.2004.09.021

Hogarth DD (2016) Chemical trends in the Meech Lake, Québec, carbonatites and fenites. Can Mineral 54(5):1105–1128. https://doi.org/10.3749/canmin.1400061

Holland TJB, Powell R (1998) An internally consistent thermodynamic data set for phases of petrological interest. J Metamorph Geol 16(3):309–343. https://doi.org/10.1111/j.1525-1314.1998.00140.x

Holland T, Powell R (2003) Activity–composition relations for phases in petrological calculations: an asymmetric multicomponent formulation. Contrib Miner Petrol 145(4):492–501. https://doi.org/10.1007/s00410-003-0464-z

Holland TJB, Powell R (2011) An improved and extended internally consistent thermodynamic dataset for phases of petrological interest, involving a new equation of state for solids. J Metamorph Geol 29(3):333–383. https://doi.org/10.1111/j.1525-1314.2010.00923.x

Hurai V, Blažeková M, Huraiová M, Siegfried PR, Slobodník M, Konečný P (2021) Thermobarometric and geochronologic constraints on the emplacement of the Neoproterozoic Evate carbonatite during exhumation of the Monapo granulite complex, Mozambique. Lithos 380–381:105883. https://doi.org/10.1016/j.lithos.2020.105883

Isakova AT, Panina LI, Rokosova EY (2015) Carbonatite melts and genesis of apatite mineralization in the Guli pluton (northern East Siberia). Russ Geol Geophys 56(3):466–475. https://doi.org/10.1016/j.rgg.2015.02.007

Káldos R, Guzmics T, Mitchell RH, Dawson JB, Milke R, Szabó C (2015) A melt evolution model for Kerimasi volcano, Tanzania: evidence from carbonate melt inclusions in jacupirangite. Lithos 238:101–119. https://doi.org/10.1016/j.lithos.2015.09.011

Kamenetsky VS, Doroshkevich AG, Elliott HAL, Zaitsev AN (2021) Carbonatites: contrasting, complex, and controversial. Elements 17(5):307–314. https://doi.org/10.2138/gselements.17.5.307

Kjarsgaard BA (1998) Phase relations of a carbonated high-CaO nephelinite at 0.2 and 0.5 GPa. J Petrolog 39(11–12):2061–2075. https://doi.org/10.1093/petroj/39.11-12.2061

Kjarsgaard BA, Hamilton DL (1988) Liquid immiscibility and the origin of alkali-poor carbonatites. Mineral Mag 52:43–55. https://doi.org/10.1180/minmag.1988.052.364.04

Kjarsgaard BA, Hamilton DL, Peterson TD (1995) Peralkaline nephelinite/carbonatite liquid immiscibility: Comparison of phase compositions in experiments and natural lavas from Oldoinyo Lengai. In: Bell K, Keller J (eds) Carbonatite volcanism, vol 4. Springer Berlin Heidelberg, Berlin, pp 163–190. https://doi.org/10.1007/978-3-642-79182-6_13

Le Bas MJ, Aspden JA (1981) The comparability of carbonatitic fluid inclusions in ijolites with natrocarbonatite lava. Bull Volcanologique 44(3):429–438. https://doi.org/10.1007/bf02600574

Le Maitre RW, Streckeisen A, Zanettin B, Le Bas MJ, Bonin B, Bateman P (2002) Igneous rocks: a classification and glossary of terms, 2nd edn. Cambridge University Press, Cambridge. https://doi.org/10.1017/cbo9780511535581

Lee WJ, Wyllie PJ (1998) Petrogenesis of carbonatite magmas from mantle to crust, constrained by the system $CaO–(MgO + FeO^*)–(Na_2O + K_2O)–(SiO_2 + Al_2O_3 + TiO_2)–CO_2$. J Petrol 39(3):495–517. https://doi.org/10.1093/petroj/39.3.495

Lee WJ, Wyllie PJ (2000) The system CaO-MgO-SiO$_2$-CO$_2$ at 1 GPa, metasomatic wehrlites, and primary carbonatite magmas. Contrib Miner Petrol 138(3):214–228. https://doi.org/10.1007/s004100050558

Li Y, Zhang J, Mostofa KMG, Wang Y, Yu S, Cai Z, Li P, Zhou G, Fu C, Mao X (2018) Petrogenesis of carbonatites in the Luliangshan region, North Qaidam, northern Tibet, China: Evidence for recycling of sedimentary carbonate and mantle metasomatism within a subduction zone. Lithos 322:148–165. https://doi.org/10.1016/j.lithos.2018.10.010

Loidolt C, Zimmermann R, Tusa L, Lorenz S, Ebert D, Gloaguen R, Broom-Fendley S (2023) New Insights into the rare earth element mineralization of the Storkwitz carbonatite, Germany. Can Mineral 60(6):913–932. https://doi.org/10.3749/canmin.2100061

Markl G, Marks MAW, Frost BR (2010) On the controls of oxygen fugacity in the generation and crystallization of peralkaline melts. J Petrol 51(9):1831–1847. https://doi.org/10.1093/petrology/egq040

Martin LHJ, Schmidt MW, Mattsson HB, Ulmer P, Hametner K, Günther D (2012) Element partitioning between immiscible carbonatite–kamafugite melts with application to the Italian ultrapotassic suite. Chem Geol 320–321:96–112. https://doi.org/10.1016/j.chemgeo.2012.05.019

Martin LHJ, Schmidt MW, Mattsson HB, Guenther D (2013) Element partitioning between immiscible carbonatite and silicate melts for dry and H$_2$O-bearing systems at 1–3 GPa. J Petrol 54(11):2301–2338. https://doi.org/10.1093/petrology/egt048

Massuyeau M, Gardés E, Morizet Y, Gaillard F (2015) A model for the activity of silica along the carbonatite–kimberlite–mellilitite–basanite melt compositional joint. Chem Geol 418:206–216. https://doi.org/10.1016/j.chemgeo.2015.07.025

Matsumoto T, Banno S (1970) A natural pyroxene with the space group C^{42h}–P2/n. Proc Jpn Acad 46(2):173–175. https://doi.org/10.2183/pjab1945.46.173

Mattsson HB, Högdahl K, Carlsson M, Malehmir A (2019) The role of mafic dykes in the petrogenesis of the Archean Siilinjärvi carbonatite complex, east-central Finland. Lithos 342–343:468–479. https://doi.org/10.1016/j.lithos.2019.06.011

Mikhailova J, Ivanyuk G, Kalashnikov A, Pakhomovsky Y, Bazai A, Panikorovskii T, Yakovenchuk V, Konopleva N, Goryainov P (2018) Three-D mineralogical mapping of the Kovdor phoscorite–carbonatite complex, NW Russia: I. Forsterite. Minerals 8(6):260. https://doi.org/10.3390/min8060260

Mitchell RH (2005) Carbonatites and carbonatites and carbonatites. Can Mineral 43(6):2049–2068. https://doi.org/10.2113/gscanmin.43.6.2049

Mitchell RH, Dawson JB (2012) Carbonate–silicate immiscibility and extremely peralkaline silicate glasses from Nasira cone and recent eruptions at Oldoinyo Lengai Volcano, Tanzania. Lithos 152:40–46. https://doi.org/10.1016/j.lithos.2012.01.006

Mollé V, Gaillard F, Nabyl Z, Tuduri J, Di Carlo I, Erdmann S (2022) Crystallisation sequence of a REE-rich carbonate melt: an experimental approach. Comptes Rendus Géosci 353(S2):217–231. https://doi.org/10.5802/crgeos.108

Moore JN, Kerrick DM (1976) Equilibria in siliceous dolomites of the Alta aureole, Utah. Am J Sci 276(4):502–524. https://doi.org/10.2475/ajs.276.4.502

Moore KR, Brady AE, Costanzo A (2022) Crystal-liquid segregation in silicocarbonatite magma leads to the formation of calcite carbonatite. J Petrol 63(7):egac056. https://doi.org/10.1093/petrology/egac056

Morogan V (1994) Ijolite versus carbonatite as sources of fenitization. Terra Nova 6(2):166–176. https://doi.org/10.1111/j.1365-3121.1994.tb00650.x

Morse SA (1970) Alkali feldspars with water at 5 kb pressure. J Petrol 11(2):221–251. https://doi.org/10.1093/petrology/11.2.221

Nadeau O, Stevenson R, Jébrak M (2016) Evolution of Montviel alkaline–carbonatite complex by coupled fractional crystallization, fluid mixing and metasomatism—part I: petrography and geochemistry of metasomatic aegirine–augite and biotite: implications for REE–Nb mineralization. Ore Geol Rev 72:1143–1162. https://doi.org/10.1016/j.oregeorev.2015.09.022

Nasir S, Hanna S, Hajari S (2003) The petrogenetic association of carbonatite and alkaline magmatism: constraints from the Masfut-Rawda Ridge, North Oman Mountains. Mineral Petrol 77(3–4):235–258. https://doi.org/10.1007/s00710-002-0198-z

Nielsen TFD, Solovova IP, Veksler IV (1997) Parental melts of melilitolite and origin of alkaline carbonatite: evidence from crystallised melt inclusions, Gardiner complex. Contrib Miner Petrol 126(4):331–344. https://doi.org/10.1007/s004100050254

Nivin VA, Treloar PJ, Konopleva NG, Ikorsky SV (2005) A review of the occurrence, form and origin of C-bearing species in the Khibiny Alkaline Igneous Complex, Kola Peninsula, NW Russia. Lithos 85(1–4):93–112. https://doi.org/10.1016/j.lithos.2005.03.021

O'Brien H, Heilimo E, Heino P (2015) The Archean Siilinjärvi carbonatite complex. In: Maier WD, Lahtinen R, O'Brien H (eds) Mineral deposits of Finland. Elsevier, Amsterdam, pp 327–343. https://doi.org/10.1016/b978-0-12-410438-9.00013-3

Otto JW, Wyllie PJ (1993) Relationships between silicate melts and carbonate-precipitating melts in CaO-MgO-SiO$_2$-CO$_2$-H$_2$O at 2 kbar. Mineral Petrol 48(2–4):343–365. https://doi.org/10.1007/bf01163107

Pdah DSM, Khonglah MA (2022) Orbicular and nodular structures in carbonatite of the Sung Valley ultramafic-alkaline-carbonatite complex, Shillong Plateau, Meghalaya, NE India: their petrogenetic implications. J Geol Soc India 98(5):635–640. https://doi.org/10.1007/s12594-022-2038-6

Plechov PY, Shcherbakov VD, Nekrylov NA (2018) Extremely magnesian olivine in igneous rocks. Russ Geol Geophys 59(12):1702–1717. https://doi.org/10.1016/j.rgg.2018.12.012

Prokof'ev VY, Seredkin MV, Zotov IA, Anoshechkina VA (2005) Genesis of magnetite–apatite and phlogopite deposits in the Kovdor Massif, Kola Peninsula: evidence from melt and fluid inclusions. Doklady Earth Sci 403(5):727–731

Prokopyev IR, Doroshkevich AG, Zhumadilova DV, Starikova AE, Nugumanova YN, Vladykin NV (2021) Petrogenesis of Zr–Nb (REE) carbonatites from the Arbarastakh complex (Aldan Shield, Russia): mineralogy and inclusion data. Ore Geol Rev 131:104042. https://doi.org/10.1016/j.oregeorev.2021.104042

Rankin AH, Le Bas MJ (1974) Liquid immiscibility between silicate and carbonate melts in naturally occuring ijolite magma. Nature 250(5463):206–209. https://doi.org/10.1038/250206a0

Reguir EP, Chakhmouradian AR, Pisiak L, Halden NM, Yang P, Xu C, Kynický J, Couëslan CG (2012) Trace-element composition and zoning in clinopyroxene- and amphibole-group minerals: implications for element partitioning and evolution of carbonatites. Lithos 128–131:27–45. https://doi.org/10.1016/j.lithos.2011.10.003

Ryabchikov ID, Kogarko LN (2009) Redox potential of the Khibiny magmatic system and genesis of abiogenic hydrocarbons in alkaline plutons. Geol Ore Deposits 51(6):425–440. https://doi.org/10.1134/s1075701509060014

Ryabchikov ID, Kogarko LN, Krivdik SG, Ntaflos T (2008) Constraints of the formation of carbonatites in the Chernigovka Massif, Azov Region, Ukraine. Geol Ore Deposits 50(6):423–432. https://doi.org/10.1134/s1075701508060019

Savard JJ, Mitchell RH (2021) Petrology of ijolite series rocks from the Prairie Lake (Canada) and Fen (Norway) alkaline rock-carbonatite complexes. Lithos 396–397:106188. https://doi.org/10.1016/j.lithos.2021.106188

Savelyeva VB, Demonterova EI, Danilova YV, Bazarova EP, Ivanov AV, Kamenetsky VS (2016) New carbonatite complex in the western Baikal area, southern Siberian craton: mineralogy, age, geochemistry, and petrogenesis. Petrology 24(3):271–302. https://doi.org/10.1134/s0869591116030061

Sekisova VS, Sharygin VV, Zaitsev AN, Strekopytov S (2015) Liquid immiscibility during crystallization of forsterite–phlogopite ijolites at Oldoinyo Lengai Volcano, Tanzania: study of melt inclusions. Russ Geol Geophys 56(12):1717–1737. https://doi.org/10.1016/j.rgg.2015.11.005

Sharygin VV, Kamenetsky VS, Zaitsev AN, Kamenetsky MB (2012) Silicate–natrocarbonatite liquid immiscibility in 1917 eruption combeite–wollastonite nephelinite, Oldoinyo Lengai Volcano, Tanzania: melt inclusion study. Lithos 152:23–39. https://doi.org/10.1016/j.lithos.2012.01.021

Shumilova TG, Isaenko SI, Divaev FK (2013) Mineralogical features of diamond, amorphous diamond-like carbon and graphite from Chagatay carbonatites (Uzbekistan). Mineral J 35(2):81–89. http://jnas.nbuv.gov.ua/article/UJRN-0000082879

Skelton A, Hode Vuorinen J, Arghe F, Fallick A (2007) Fluid–rock interaction at a carbonatite-gneiss contact, Alnö, Sweden. Contrib Mineral Petrol 154(1):75–90. https://doi.org/10.1007/s00410-007-0180-1

Slezak P, Spandler C, Border A, Whittock K (2021) Geology and ore genesis of the carbonatite-associated Yangibana REE district, Gascoyne Province, Western Australia. Miner Deposita 56(5):1007–1026. https://doi.org/10.1007/s00126-020-01026-z

Smith MR (2017) ms609/Ternary: v2.3.0. Zenodo. https://doi.org/10.5281/zenodo.1068996

Stoppa F (2021) Evolution and involution of carbonatite thoughts. Elements 17(5):303–304. https://doi.org/10.2138/gselements.17.5.303

Stoppa F, Schiazza M, Rosatelli G, Castorina F, Sharygin VV, Ambrosio FA, Vicentini N (2019) Italian carbonatite system: from mantle to ore-deposit. Ore Geol Rev 114:103041. https://doi.org/10.1016/j.oregeorev.2019.103041

Su K, Zhang S-B, Li Z-X, Zhang L, Liang T, Du Y, Li L (2023) When carbonatite met granite: a carbonatite magma- wall rock reaction origin for the Paleoproterozoic pyroxenite and syenite in Fengzhen, North China. Lithos 454–455:107231. https://doi.org/10.1016/j.lithos.2023.107231

Ting W, Burke EAJ, Rankin AH, Woolley AR (1994) Characterisation and petrogenetic significance of CO_2, H_2O and CH_4 fluid inclusions in apatite from the Sukulu carbonatite, Uganda. Eur J Mineral 6(6):787–804. https://doi.org/10.1127/ejm/6/6/0787

Tracy RJ, Frost BR (1991) Phase equilibria and thermobarometry of calcareous, ultramafic and mafic rocks, and iron formations. Rev Mineral 26(1):207–289. https://doi.org/10.2138/rmg.1991.26.5

Tsujimori T (2005) Coexisting retrograde jadeite and omphacite in a jadeite-bearing lawsonite eclogite from the Motagua Fault Zone, Guatemala. Am Mineral 90(5–6):836–842. https://doi.org/10.2138/am.2005.1699

Vasyukova OV, Williams-Jones AE (2022) Carbonatite metasomatism, the key to unlocking the carbonatite-phoscorite-ultramafic rock paradox. Chem Geol 602:120888. https://doi.org/10.1016/j.chemgeo.2022.120888

Vasyukova OV, Williams-Jones AE (2023) A new model for the origin of pyrochlore: evidence from the St Honoré Carbonatite, Canada. Chem Geol 632:121549. https://doi.org/10.1016/j.chemgeo.2023.121549

Vasyukova O, Kostyuk A, Williams-Jones A (2023) Kovdor to Oldoinyo Lengai—the missing link in carbonatitic magma evolution. Geology 51(1):59–63. https://doi.org/10.1130/g50672.1

Veksler IV, Lentz D (2006) Parental magmas of plutonic carbonatites, carbonate–silicate immiscibility and decarbonation reactions: evidence from melt and fluid inclusions. In: Webster JD (ed) Melt inclusions in plutonic rocks, vol 36. Mineralogical Association of Canada, Montreal, pp 123–149

Veksler IV, Nielsen TFD, Sokolov SV (1998) Mineralogy of crystallized melt inclusions from Gardiner and Kovdor ultramafic alkaline complexes: implications for carbonatite genesis. J Petrol 39(11–12):2015–2031. https://doi.org/10.1093/petroj/39.11-12.2015

Veksler IV, Dorfman AM, Dulski P, Kamenetsky VS, Danyushevsky LV, Jeffries T, Dingwell DB (2012) Partitioning of elements between silicate melt and immiscible fluoride, chloride, carbonate, phosphate and sulfate melts, with implications to the origin of natrocarbonatite. Geochim Cosmochim Acta 79:20–40. https://doi.org/10.1016/j.gca.2011.11.035

Ventura GD, Redhammer GJ, Galdenzi F, Ventruti G, Susta U, Oberti R, Radica F, Marcelli A (2023) Oxidation or cation re-arrangement? Distinct behavior of riebeckite at high temperature. Am Miner 108(1):59–69. https://doi.org/10.2138/am-2022-8073

Viladkar SG (2017) Pyroxene-sövite in Amba Dongar carbonatite-alkalic complex, Gujarat. J Geol Soc India 90(5):591–594. https://doi.org/10.1007/s12594-017-0756-y

Viladkar SG (2019) Silico-carbonatite vs silicified carbonatite in Amba Dongar carbonatite diatreme, Gujarat, India. J Geol Soc India 94(5):548–549. https://doi.org/10.1007/s12594-019-1355-x

Walter BF, Giebel RJ, Steele-MacInnis M, Marks MAW, Kolb J, Markl G (2021) Fluids associated with carbonatitic magmatism: a critical review and implications for carbonatite magma ascent. Earth Sci Rev 215:103509. https://doi.org/10.1016/j.earscirev.2021.103509

Warr LN (2021) IMA–CNMNC approved mineral symbols. Mineral Mag 85(3):291–320. https://doi.org/10.1180/mgm.2021.43

Wei C-W, Xu C, Chakhmouradian AR, Brenna M, Kynicky J, Song W-L (2020) Carbon–strontium isotope decoupling in carbonatites from Caotan (Qinling, China): implications for the origin of calcite carbonatite in orogenic settings. J Petrol 61(2):egaa024. https://doi.org/10.1093/petrology/egaa024

Weidendorfer D, Asimow PD (2022) Experimental constraints on truly conjugate alkaline silicate—carbonatite melt pairs. Earth Planet Sci Lett 584:117500. https://doi.org/10.1016/j.epsl.2022.117500

Weidendorfer D, Schmidt MW, Mattsson HB (2017) A common origin of carbonatite magmas. Geology 45(6):507–510. https://doi.org/10.1130/g38801.1

White RW, Powell R, Clarke GL (2002) The interpretation of reaction textures in Fe-rich metapelitic granulites of the Musgrave Block, central Australia: constraints from mineral equilibria calculations in the system K_2O–FeO–MgO–Al_2O_3–SiO_2–H_2O–TiO_2–Fe_2O_3. J Metamorph Geol 20(1):41–55. https://doi.org/10.1046/j.0263-4929.2001.00349.x

White RW, Powell R, Holland TJB, Johnson TE, Green ECR (2014) New mineral activity-composition relations for thermodynamic calculations in metapelitic systems. J Metamorph Geol 32(3):261–286. https://doi.org/10.1111/jmg.12071

Williams-Jones AE, Palmer DAS (2002) The evolution of aqueous–carbonic fluids in the Amba Dongar carbonatite, India: implications for fenitisation. Chem Geol 185(3–4):283–301. https://doi.org/10.1016/s0009-2541(01)00409-0

Witt WK, Hammond DP, Hughes M (2019) Geology of the Ngualla carbonatite complex, Tanzania, and origin of the Weathered Bastnaesite Zone REE ore. Ore Geol Rev 105:28–54. https://doi.org/10.1016/j.oregeorev.2018.12.002

Woolley AR (2003) Igneous silicate rocks associated with carbonatites: their diversity, relative abundances and implications for carbonatite genesis. Periodico Di Mineralogia 72(1):9–17. https://www.dst.uniroma1.it/riviste/permin/spVol1_03.html

Wu F-Y, Mitchell RH, Li Q-L, Zhang C, Yang Y-H (2017) Emplacement age and isotopic composition of the Prairie Lake carbonatite

complex, Northwestern Ontario, Canada. Geol Mag 154(2):217–236. https://doi.org/10.1017/s0016756815001120

Xie Y, Qu Y, Zhong R, Verplanck PL, Meffre S, Xu D (2019) The ~1.85 Ga carbonatite in north China and its implications on the evolution of the Columbia supercontinent. Gondwana Res 65:125–141. https://doi.org/10.1016/j.gr.2018.10.001

Yagi K (1966) The system acmite-diopside and its bearing on the stability relations of natural pyroxenes of the acmite-hedenbergite-diopside series. Am Mineral 51(7):976–1000

Yaxley GM, Anenburg M, Tappe S, Decree S, Guzmics T (2022) Carbonatites: classification, sources, evolution, and emplacement. Annu Rev Earth Planet Sci 50(1):261–293. https://doi.org/10.1146/annurev-earth-032320-104243

Zaitsev A, Polezhaeva L (1994) Dolomite-calcite textures in early carbonatites of the Kovdor ore deposit, Kola peninsula, Russia: their genesis and application for calcite-dolomite geothermometry. Contrib Miner Petrol 115(3):339–344. https://doi.org/10.1007/bf00310772

Zhang W, Terry Chen W, Zhang X-C, Tang Y-W (2022) The trace element chemistry of quartz in carbonatite-related REE deposits: implication for REE exploration. Ore Geol Rev 149:105068. https://doi.org/10.1016/j.oregeorev.2022.105068

Zhao S, Poli S, Schmidt MW, Rinaldi M, Tumiati S (2022) An experimental determination of the liquidus and a thermodynamic melt model in the $CaCO_3$-$MgCO_3$ binary, and modelling of carbonated mantle melting. Geochim Cosmochim Acta 336:394–406. https://doi.org/10.1016/j.gca.2022.08.014

Zheng X, Liu Y, Smith MP, Kynický J, Hou Z (2023) Carbonatitic magma fractionation and contamination generate rare earth element enrichment and mineralization in the Maoniuping giant REE deposit, SW China. J Petrol. https://doi.org/10.1093/petrology/egad037